

Exploratory Hidden Markov Factor Models for Longitudinal Mobile Health Data: Application to Adverse Posttraumatic Neuropsychiatric Sequelae

Lin Ge, Xinming An, Donglin Zeng,
Samuel McLean, Ronald Kessler, and Rui Song*

Abstract

Adverse posttraumatic neuropsychiatric sequelae (APNS) are common among veterans and millions of Americans after traumatic events and cause tremendous burdens for trauma survivors and society. Many studies have been conducted to investigate the challenges in diagnosing and treating APNS symptoms. However, progress has been limited by the subjective nature of traditional measures. This study is motivated by the objective mobile device data collected from the Advancing Understanding of Recovery after trauma (AURORA) study. We develop both discrete-time and continuous-time exploratory hidden Markov factor models to model the dynamic psychological conditions of individuals with either regular or irregular measurements. The proposed models extend the conventional hidden Markov models to allow high-dimensional data and feature-based nonhomogeneous transition probability between hidden psychological states. To find the maximum likelihood estimates, we develop a Stabilized Expectation-Maximization algorithm with Initialization Strategies (SEMIS). Simulation studies with synthetic data are carried out to assess the performance of parameter estimation and model selection. Finally, an application to the AURORA data is conducted, which captures the relationships between heart rate variability, activity, and APNS consistent with existing literature.

Keywords: Continuous-Time Hidden Markov Model, Discrete-Time Hidden Markov Model, Multinomial Logistic Model, Multivariate Longitudinal Data, Mental Health

*Lin Ge is graduate student (E-mail: lge@ncsu.edu) and Rui Song is Professor (rsong@ncsu.edu), Department of Statistics, North Carolina State University, Raleigh, NC 27695. Xinming An (E-mail: Xinming_An@med.unc.edu) is Research Assistant Professor, Department of Anesthesiology, The University of North Carolina at Chapel Hill, Chapel Hill, NC 27514. Donglin Zeng is Professor (E-mail: dzeng@bios.unc.edu), Department of Biostatistics, The University of North Carolina at Chapel Hill, Chapel Hill, NC 27599. Samuel McLean is Professor (E-mail: samuel_mclean@med.unc.edu), Department of Psychiatry, The University of North Carolina at Chapel Hill, Chapel Hill, NC 27514. Ronald Kessler is Professor (E-mail: kessler@hcp.med.harvard.edu), Department of Health Care Policy, Harvard Medical School, Boston, MA 02115. The research is partially supported by NSF under Grant DMS-1555244 and 2113637, NIMH under Grant U01MH110925, the US Army Medical Research and Materiel Command, The One Mind Foundation, and The Mayday Fund.

1 Introduction

Adverse posttraumatic neuropsychiatric sequelae (APNS), such as pain, depression, and PTSD, are epidemic among more than 2.5 million veterans. These disorders are also common in millions of Americans after traumatic events, such as motor vehicle collisions and sexual assault. Leading to various issues (such as disability and substance abuse) for veterans and civilian trauma survivors, the APNS causes tremendous burdens nationally.

There are three major issues related to the assessment, diagnosis, and treatment of APNS. First, these APNS have been assessed mainly based on subjective self-report measures, which are unreliable. Second, commonly used clinical diagnostic criteria/cutoffs (such as DSM IV) are arbitrary in nature, and the corresponding patients are very heterogeneous. Last, these APNS symptoms are often studied and treated separately, while many of them are often co-occurring (McLean et al., 2020). These issues greatly slowed the identification of objective markers, development of risk prediction tools and preventive/treatment interventions, and the advance in understanding the neurobiological mechanisms. During the past several decades, these difficulties have been studied extensively. However, very little progress has been made. Such is the initiative of the Advancing Understanding of RecOvery afteR traumA (AURORA) study¹ (McLean et al., 2020).

AURORA is a large-scale emergency department (ED)-based study ($n = 5000$ target sample) that uses adaptive sampling methods to collect a combination of genomics, neuroimaging, psychophysical, physiological, neurocognitive, mobile device, and self-reported data from trauma survivors. Among them, data collected from personal mobile devices, such as smartphones and smartwatches, provides a fresh way to understand people's be-

¹It is developed by the National Institutes of Mental Health, the US Army Medical Research and Material Command, the One Mind Foundation, the Stanley Center for Psychiatric Research, and the Mayday Fund, together with corporate partners including Verily Life Sciences and Mindstrong Health.

havior, mood, and health (Insel, 2017). Unlike traditionally used subjective assessments for a mood disorder, mobile device data is objectively measured and recorded. Furthermore, by capturing ecological information continuously, mobile device data can monitor individuals' real-time physiological and emotional changes when interacting with the real-life environment, which strongly affects psychological conditions.

Motivated by the potential of the enormous mobile device data collected from the AURORA study, the purpose of this work is to mitigate the issues we discussed previously related to APNS by (i) identifying homogeneous latent states based on objective mobile device data, and (ii) investigating the transition pattern between latent states. Many studies have been conducted to address the heterogeneity issue and identify homogeneous subgroups for APNS. However, most of these studies are based on either self-report survey data or neuroimaging data (Marquand et al., 2016). To our knowledge, the current study is the first to address this issue based on mobile device data. To achieve these goals, we develop two models based on the hidden Markov model (HMM) framework.

HMM is firstly developed by Baum and Petrie in 1960s (Baum and Petrie, 1966), and reviewed comprehensively in the book *Inference in hidden Markov models* (Cappé et al., 2006). HMM has been widely used in different fields. However, there are two unique challenges for mobile device data that standard HMM cannot handle, including high-dimensional spaces and irregularly spaced measurements.

First, mobile devices collect a large amount of high-dimensional data from different sensors. For example, in the AURORA study, smartwatches collect activity (accelerometer sensor) and heart rate (photoplethysmography sensor) data, while smartphones collect GPS, keystrokes, language, and communication data. After that, hundreds of features are derived from these data. For example, ten activity features, around 30 heart rate features,

more than 100 language features and almost 1000 keystroke features are derived. Therefore, dimensionality reduction is necessary.

Recently, HMM has been extended to handle high-dimensional data by incorporating the factor analysis model (FM) (Kim and Mueller, 1978) in different ways. Among them, the factor analyzed hidden Markov model (Rosti and Gales, 2002) combines an FM with a discrete-time HMM (DTHMM) (Vermunt et al., 1999). It has been widely used to address various real problems, such as speech recognition (Rosti and Gales, 2004), environmental protection (Maruotti et al., 2017), and seizure detection (Madadi, 2019). Similarly, Liu and Chen (2016) introduced the regime-switching factor model to handle high-dimensional financial market data. However, they all assume a time-homogeneous transition probability matrix and focus on a single subject instead of multiple subjects.

Song et al. (2017) developed a hidden Markov latent variable model (HMLV) to model the latent discrete process of cocaine addiction of multiple patients. However, it is not directly applicable to mobile device data. First, the HMLV uses a confirmatory factor model (CFM) with both the number of factors and the structure for the factor loading matrix pre-specified, whereas mobile device data lacks such previous knowledge. As a result, an exploratory factor model (EFM) is needed to explore the number of factors and the factor structure. Second, using the continuation-ratio logit model, the HMLV assumes the states are ordered, which is not appropriate in the present application.

Second, mobile device data collected from the real-world open environment is irregularly spaced. For example, activity and heart rate data were collected only when the participants wore the watch. As a result, each participant’s mobile device data will not be equally spaced, and different participants may have very different sampling schedules. However, all of the frameworks discussed above are based on DTHMM, which assumes evenly spaced

measurements and hence ignores the influence of time gaps between consecutive observations on the transition rate. Recently, to tackle the issue of irregularly spaced measurements, studies started considering using continuous-time discrete-state HMM (CTHMM), which allows observations to arrive at arbitrary times (Cox and Miller, 2017). CTHMM and its direct extensions, examining the effects of the covariates on transition rate, are widely used in applications in medical research involving irregularly sampled clinical measurements (Cook et al., 2002; Titman, 2011; Liu et al., 2015; Amoros et al., 2019; Zhou et al., 2020). However, none of them focus on high-dimensional data.

Thus, all the above methods cannot be used to construct a satisfactory framework for analyzing the AURORA data. Our goal is to find a model that can address both the high-dimensionality challenge and the irregular measurement schedules at the same time. In addition, we want a transition model that is simple to interpret at the population level and to include static/time-varying contextual features, such as age and gender, as covariates.

Our contributions can be summarized as follows. First, we explore the usefulness of mobile device data for mental health research. In recent years, utilizing mobile device data for health research is becoming increasingly popular across different fields. However, very few studies have been conducted on data collected from consumer-grade mobile devices in an open environment. To the best of our knowledge, this is the first large-scale extensive study in psychiatry to investigate the potential utility of mobile device data for health research. Second, to address the unique challenges introduced by mobile device data, we proposed two exploratory HMM depicting the stochastic Markov process of multiple individuals' psychological conditions simultaneously. While the discrete-time exploratory factor analyzed HMM (DT-EHMFH) assumes consistent time intervals between every two consecutive observations, the continuous-time exploratory hidden Markov factor model (CT-EHMFH) is

a more general model accepting different structures of longitudinal data that are regularly or irregularly collected. Within each model, an appropriate transition model is included to investigate how the transition probabilities are affected by contextual information. Third, we develop a Stabilized Expectation-Maximization algorithm with Initialization Strategies (SEMIS), which is presented along with detailed derivations. Simulation studies with synthetic data demonstrate outstanding parameter estimation and model selection performance. Finally, we perform a detailed analysis of the AURORA data, accompanied by interpretations and discussions of biological findings, which show the great potential of the proposed methods and mobile health data in providing more reliable diagnostics.

The outline of our article is as follows. Section 2 describes the AURORA dataset and the setup of the proposed model. Section 3 illustrates the SEMIS algorithm we used to estimate parameters. Results of a simulation study are presented in Section 4 to investigate the performance of the proposed model. In Section 5, a comprehensive real analysis of the AURORA data is reported. Finally, we conclude the paper with a discussion in Section 6.

2 Methodology

2.1 Description of AURORA Data

In the AURORA study (McLean et al., 2020), trauma survivors aged 18 to 75 who present to participating EDs within 72 hours of trauma exposure are screened for enrollment eligibility. Motor vehicle collisions (MVC), physical assault, sexual assault, falls >10 feet, or mass casualty incidents are automatically qualified for enrollment. Major exclusion criteria include administration of general anesthesia, long bone fractures, laceration with significant hemorrhage, visual or auditory impairment precluding completion of web-based

neurocognitive evaluations and/or telephone follow-ups, prisoners, pregnant or breastfeeding, ongoing domestic violence. To be eligible for the study, patients need to be fluent in written and spoken English and have an iOS/Android smartphone with internet access.

The AURORA study initially focuses on trauma survivors who present to EDs and are discharged home after evaluation but subsequently also recruits a subsample of patients admitted for no more than 24 hours (as of April 4, 2018) and then for no more than 72 hours (as of December 11, 2018). Participants used here are from the third data freeze, which includes participants who were enrolled at least up to day 67 of the study. Participants who became pregnant, incarcerated, or deceased during the tenure are excluded.

For the current research, we mainly focus on heart rate variability (HRV) and activity features extracted from PPG and accelerometer data collected from Verily’s smartwatches in the first 100 days after enrolling in the AURORA study, as previous research has suggested that HRV and activity features are associated with APNS (Hartmann et al., 2019; Jung et al., 2019). Activity features are extracted on a 24-hour window to evaluate the daily activity patterns of the participants. After converting accelerometer data to activity counts, the mean and standard deviation of activity counts are calculated for each 24-hour period. Additionally, cosinor rhythmometry features were derived to capture circadian rhythm. HRV features were derived by first calculating the beat-to-beat (BB) interval (Shaffer and Ginsberg, 2017) time series from PPG data. Afterward, noises are identified and removed from BB interval time series to derive normal-to-normal (NN) interval time series. Finally, a 5-minute window with a 30-second sliding step was used to analyze the NN interval time series to derive HRV features. In the following subsections, we will further discuss the activity data and HRV data, and end up with a description of the final dataset of our interest.

2.1.1 Activity Features

The meanAcc and the stdAcc are the mean and the standard deviation of the activity counts calculated by the approach described in Borazio et al. (2014), serving as descriptive statistics about the level of activity in the given time period. The amplitude is a feature derived from the Cosinor Rhythmometry Analysis (Cornelissen, 2014) to quantify circadian rhythm. Applying the Cole-Kripke algorithm (Cole et al., 1992) on accelerometry epochs, each epoch is classified as wake or sleep. The SWCK is the number of transitions between wake epochs and sleep epochs divided by data length. Based on the raw accelerometer data (Van Someren et al., 1999), the average activity over the least active five hours (L5) is obtained, indicating the nighttime activity.

2.1.2 Heart Rate Features

Technically, HRV features can be grouped into three sets consisting of time-domain measures, frequency-domain measures, and nonlinear measures (Shaffer and Ginsberg, 2017). For this study, we selected seven heart rate features to measure the average, variability, and complexity of the heart rate time series.

NNmean is the average heart rate, while the NNskew and SDNN are the skewness and standard deviation of the normal-to-normal interval (Shaffer and Ginsberg, 2017), respectively. In particular, higher skewness indicates rapid accelerations or decelerations. LfHF is the ratio of the low-frequency power and high-frequency power. According to Shaffer and Ginsberg (2017), a low LfHF ratio suggests parasympathetic dominance (i.e., engage in tend-and-befriend behaviors), whereas a high LfHF ratio shows sympathetic dominance (i.e., engage in fight-or-flight behaviors). DC is a predictor of mortality in heart attack survivors, according to Kantelhardt et al. (2007). The lower the DC index, the higher the

risk of mortality. The rest two variables characterize the time intervals between consecutive heartbeats (R-R interval). While SD1SD2 assesses the unpredictability of a time series of R-R intervals, ApEn measures the regularity and complexity. A big ApEn shows R-R interval volatility, whereas a small ApEn indicates a steady and predictable temporal sequence of R-R intervals (Shaffer and Ginsberg, 2017).

To align with the activity data, we summarize an individual’s daily HRV data by including only daily statistical summaries of each HRV feature, such as mean, median, minimum, maximum, kurtosis, skewness, interquartile range, and standard deviation.

2.1.3 Datasets

The final dataset we used included observations collected from 258 patients, each having a different number of total daily records ranging from 17 to 99. Note that observations in this dataset are irregularly sampled. Therefore, a subset of it, including only observations collected at {day 2, day 12, \dots , day 82}, is also of our interest. In the subset with systematic observations, 180 patients are included. Based on domain knowledge, 23 variables are of our main interest. Four of them are derived from the activity data, while the remaining 19 are derived from the HRV data. Besides, the transition model includes both age (range from 18-74) and gender (0-male, 1-female) to investigate the effect of age and gender on the transition probabilities. There are more details about the data preparation in Section B of the supplementary article.

2.2 Exploratory Hidden Markov Factor Model (EHMFM)

Motivated by the data structure of the processed AURORA datasets, we consider data in the form of repeated measurements of p features over time T_i for each individual i of N

subjects. The model is in the framework of HMM, which models the Markov process of individuals' longitudinal responses. Let w_{it} be the latent state of individual i at occasion t , taking value from the finite discrete set $\{1, \dots, J\}$. Here, J is the total number of states, which is assumed to be known and fixed. Let $\mathbf{W}_i = (w_{i1}, \dots, w_{iT_i})$ be the state sequence over T_i repeated measurements. Let a $J \times J$ matrix \mathbf{P}_{it} be the transition probability matrix for individual i at occasion t , $t = \{2, \dots, T_i\}$, of which the (k, j) entry is

$$\mathbf{P}_{it,kj} = P(w_{it} = j | w_{i,t-1} = k), \quad (1)$$

and $\mathbf{P}_{it,kk} = 1 - \sum_{j=1}^J \mathbf{P}_{it,kj}$. When $t = 1$, we assume the initial state follows a multinomial distribution with probabilities $\boldsymbol{\pi} = (\pi_1, \dots, \pi_J)'$, where $\sum_{i=1}^J \pi_i = 1$. HMM aims to specify a latent Markov process given observations by estimating the transition probability matrix \mathbf{P} and the initial state distribution.

Additionally, unlike the conventional HMM, our model considers two extra parts to address the unique challenges and achieve our goals. In the first part, discussed in Section 2.2.1, we assume a state-specific measurement model of the observations to reduce dimensionality by utilizing the FM. In the second part, discussed in Section 2.2.2, we introduce different transition models to both the discrete-time version and the continuous-time version of our model. Typically, conventional HMM assumes constant transition probabilities, which can be easily violated when analyzing multiple individuals simultaneously. Therefore, our model considers individual-specific and time-specific transition probabilities by involving a transition model. Furthermore, within Section 2.2.2, considering the continuous-time version, we further tackle the issue of irregular spacing.

2.2.1 State-Specific Measurement Model

Let \mathbf{y}_{it} denote a $p \times 1$ vector of the observed value of p outcome variables for subject i at time t , where $i = 1, \dots, N$ and $t = 1, \dots, T_i$. Let \mathbf{z}_{it} be a K dimensional vector of latent scores independent of w_{it} and following a standard multivariate normal distribution. K is assumed to be the same across states here, however, our model can simply be extended to the version with different K_j . For each individual i , $\mathbf{Y}_i = (\mathbf{y}_{i1}, \dots, \mathbf{y}_{iT})$ is a $p \times T$ matrix containing all measurements of individual i over time and $\mathbf{Z}_i = (\mathbf{z}_{i1}, \dots, \mathbf{z}_{iT})$ is a $K \times T$ matrix containing all latent features of individual i over time.

The first part of our model is an FM, which aims to find a lower number of latent variables to describe the variability among high-dimensional response variables. Considering individual i at time t , suppose $w_{it} = j$, then the FM assumes a state-specific measurement model as the following:

$$[\mathbf{y}_{it}|w_{it} = j] = \boldsymbol{\mu}_j + \boldsymbol{\Lambda}_j \mathbf{z}_{it} + \mathbf{e}_{it}; \quad \mathbf{z}_{it} \stackrel{i.i.d.}{\sim} \mathcal{N}(\mathbf{0}, \mathbf{I}_K), \mathbf{e}_{it} \stackrel{i.i.d.}{\sim} \mathcal{N}(\mathbf{0}, \boldsymbol{\Psi}), \mathbf{z}_{it} \perp\!\!\!\perp \mathbf{e}_{it} \quad (2)$$

where $\boldsymbol{\mu}_j$ is a $p \times 1$ vector of state-specific expected mean response, $\boldsymbol{\Lambda}_j$ is a $p \times K$ state-specific factor loading matrix, $\boldsymbol{\Psi}$ is a $p \times p$ diagonal covariance matrix for the error term \mathbf{e}_{it} with positive nonconstant diagonal entries. In addition to the normality assumption made on both \mathbf{z}_{it} and \mathbf{e}_{it} , we assume independence between \mathbf{z}_{it} and \mathbf{e}_{it} . Therefore, an alternative way to represent the state-specific measurement model is as follows:

$$[\mathbf{y}_{it}|w_{it} = j] \stackrel{i.i.d.}{\sim} \mathcal{N}(\boldsymbol{\mu}_j, \boldsymbol{\Lambda}_j \boldsymbol{\Lambda}_j' + \boldsymbol{\Psi}). \quad (3)$$

2.2.2 Transition Model

Considering the two data structures discussed in Section 2.1, different transition models are needed for different data. In the following, we first illustrate unique components in the DT-EHMF, which ignores the effects of time intervals between two consecutive observations, to get a brief understanding of the structure of the proposed integrating model. In other words, the DT-EHMF assumes consistent time intervals between measurements, which is easy to be violated in digital health data. Then, we further introduce the CT-EHMF, which allows longitudinal data collected on a regular or irregular basis to relax the assumption of identical time intervals.

DT-EHMF: Given a state sequence \mathbf{W}_i , standard assumptions of DTHMM assume that 1) given a state w_{it} , observations \mathbf{y}_{it} are independent, and 2) given a state w_{it} and subjects' contextual features, the state at the next occasion $w_{i,t+1}$ is not related to any information from previous occasions.

Utilizing subjects' contextual information, we use a multinomial logistic regression model to explicitly characterize the transition probability matrix \mathbf{P}_{it} as follows:

$$\log\left(\frac{\mathbf{P}_{it,kj}|\mathbf{x}_{it}}{\mathbf{P}_{it,kk}|\mathbf{x}_{it}}\right) = \mathbf{x}'_{it}\mathbf{B}_{kj}, \quad t = \{2, \dots, T_i\}, \quad (4)$$

where \mathbf{x}_{it} is a $d \times 1$ vector of vector of covariates for individual i at time t , and \mathbf{B}_{kj} is a state-specific $d \times 1$ vector of fixed effects coefficients. Here, \mathbf{x}_{it} can be reduced to \mathbf{x}_i , which contains only baseline features. The \mathbf{B}_{kj} intends to quantify the effect of covariates on the probability of transitioning from state k to another different state j , and provide an interpretation of how the probability of persisting in a state is affected by covariates. Conventionally, $\mathbf{B}_{kk} = \mathbf{0}$.

However, when directly using DT-EHMFMM on irregularly spaced datasets, we must always be careful when interpreting the predicted transition model. With irregularly sampled temporal data, multiple complex transitions can occur between any two consecutive observations. Intuitively, given w_{it} , the distribution of $w_{i,t+1}$ intends to approach a uniform distribution as observation intervals lengthen. Extra bias will be introduced when directly using the DT-EHMFMM on the dataset with different time intervals.

CT-EHMFMM: Unlike the DTHMM, which requires the time intervals to equal, the CTHMM relaxes such a requirement by taking the effects of the time interval into account. Thus, instead of directly depending on the transition probability matrix \mathbf{P} , the continuous-time Markov process is characterized by a transition intensity matrix \mathbf{Q} (Albert, 1962), which is the limits of the transition probability matrix \mathbf{P} as the time interval goes to 0.

Suppose δ_{it} is the number of pre-specified time units between t^{th} and $(t-1)^{th}$ observation, then the transition intensity for subject i from j to k at time t is

$$q_{jk} = \lim_{\delta_{it} \rightarrow 0} \frac{P(w_{it} = k | w_{i,t-\delta_{it}} = j)}{\delta_{it}} > 0, j \neq k, \quad (5)$$

and $q_{jj} = -\sum_{k \neq j} q_{jk}$, $j, k = 1, \dots, J$. The corresponding transition probability matrix $\mathbf{P}(\delta_{it})$ can be calculated as the matrix exponential of $\delta_{it} * \mathbf{Q}$. We assume that the time intervals are independent, and \mathbf{Q} is independent of time.

To explore the covariates effect on the transition rates, the transition intensity matrix can be modeled through a log linear model (Cook et al., 2002; Habtemichael et al., 2018),

$$\log(q_{jk}) | \mathbf{x}_{it} = \mathbf{x}'_{it} \mathbf{B}_{jk}. \quad (6)$$

Although the CT-EHMFMM is much more general than the DT-EHMFMM, computing the

exponential of a matrix can be difficult. For the sake of simplicity, we approximate the $\exp(\mathbf{Q})$ by using the $(\mathbf{I} + \mathbf{Q}/a)^a$ for some sufficiently large a (Ross et al., 1996).

3 SEMIS Algorithm

Let $\boldsymbol{\lambda} = (\{\boldsymbol{\mu}_j\}_{j=1}^J, \{\boldsymbol{\Lambda}_j\}_{j=1}^J, \boldsymbol{\Psi}, \{\mathbf{B}_{kj}\}_{k,j=1}^J, \boldsymbol{\pi})$. For each individual i , suppose the sequence of latent states \mathbf{W}_i and the latent factor scores \mathbf{Z}_i are given. Since we assume the state sequence holds the Markov property and \mathbf{y}_{it} is independent conditional on w_{it} , we have the following probability joint distribution of the observations and all latent variables:

$$L_{ci}(\boldsymbol{\lambda}) = P(w_{i1}) \times \prod_{t=2}^{T_i} P(w_{it}|w_{i,t-1}, \mathbf{x}_{it}) \times \prod_{t=1}^{T_i} P(\mathbf{y}_{it}|w_{it}, \mathbf{z}_{it})P(\mathbf{z}_{it}), \quad (7)$$

which is also known as the complete likelihood function with full information for individual i . By the independence property of \mathbf{Y}_i , \mathbf{W}_i , and \mathbf{Z}_i across i , the complete likelihood function (L_c) for the whole sample is obtained by taking the product of equation(7) over i .

Our goal is to estimate $\boldsymbol{\lambda}$ by maximizing the likelihood function L_c , or equivalently, maximizing its logarithm l_c . Since both \mathbf{W}_i and \mathbf{Z}_i are unobserved, it is common to implement the expectation-maximization (EM) algorithm to find the maximum likelihood estimator (MLE). As the name suggests, the EM algorithm finds a local maximum of the marginal likelihood by iteratively applying the expectation step and the maximization step, which will be discussed in the following.

3.1 Expectation Step (E-step)

In this step, we are interested in getting the expectation of l_c given observations, with respect to the current conditional distribution of unobserved variables and the current

parameter estimates $\boldsymbol{\lambda}^v$. Denote the target expectation (i.e., $E_{\boldsymbol{\lambda}^v}[l_c(\boldsymbol{\lambda})|\mathbf{Y}, \mathbf{X}]$) as $\Omega(\boldsymbol{\lambda}, \boldsymbol{\lambda}^v)$. While there is an explicit form of the probability density function of latent factor z_{it} under the assumption of normal distribution, the calculation of conditional state probabilities can be computationally heavy. Therefore, a scaled version of the forward-backward algorithm (FBA) (Rabiner, 1989) is used to get the conditional state probabilities efficiently. Note that the E-step is almost the same for both DT-EHMF and CT-EHMF, except for the dependence of $\mathbf{P}_{it,kj}$ on δ_{it} in CT-EHMF.

Firstly, we define the forward probability $\alpha_{ij}(t)$ as $P(w_{it} = j|\mathbf{y}_{i1}, \dots, \mathbf{y}_{it})$. Denote $P_j(\mathbf{y}_{it})$ the probability density function of the conditional distribution of \mathbf{y}_{it} given state j and $c_i(t)$ the conditional probability of observation \mathbf{y}_{it} given all past observations (i.e., $P(\mathbf{y}_{it}|\mathbf{y}_{i1}, \dots, \mathbf{y}_{i,t-1}, \boldsymbol{\lambda})$). For each individual $i \in \{1, \dots, N\}$ and each state $j \in \{1, \dots, J\}$, using a recursion scheme, the forward probabilities at $t \in \{1, \dots, T_i\}$ will be calculated as:

$$\alpha_{ij}(1) = \frac{\pi_j P_j(\mathbf{y}_{i1})}{\sum_{j=1}^J \pi_j P_j(\mathbf{y}_{i1})} = \frac{\pi_j P_j(\mathbf{y}_{i1})}{c_i(1)}; \quad (8)$$

$$\alpha_{ij}(t) = \frac{P_j(\mathbf{y}_{it})[\sum_{k=1}^J \alpha_{ik}(t-1)\mathbf{P}_{itkj}]}{\sum_{j=1}^J P_j(\mathbf{y}_{it})[\sum_{k=1}^J \alpha_{ik}(t-1)\mathbf{P}_{itkj}]} = \frac{P_j(\mathbf{y}_{it})[\sum_{k=1}^J \alpha_{ik}(t-1)\mathbf{P}_{itkj}]}{c_i(t)}. \quad (9)$$

Secondly, we define the backward probability $\beta_{ij}(t)$ as $\frac{P(\mathbf{y}_{i,t+1}, \dots, \mathbf{y}_{i,T_i}|w_{it}=j, \boldsymbol{\lambda})}{c_i(t+1)}$. Similarly, we define a recursion form to update the backward probabilities at $t \in \{1, \dots, T_i\}$ as follows:

$$\beta_{ij}(T_i) = 1, \quad \beta_{ij}(t) = \frac{\sum_{k=1}^J \mathbf{P}_{i,t+1,jk} P_k(\mathbf{y}_{i,t+1}) \beta_{ik}(t+1)}{c_i(t+1)}. \quad (10)$$

Thirdly, in the smoothing step, denote $\epsilon_{ikj}^v(t)$ as $P(w_{i,t} = j, w_{i,t-1} = k|\mathbf{Y}_i, \boldsymbol{\lambda}^v)$ and $\gamma_{ij}^v(t)$ as $P(w_{it} = j|\mathbf{Y}_i, \boldsymbol{\lambda}^v)$. The target conditional state probabilities are functions of the forward

probability and backward probability as follows:

$$\gamma_{ij}^v(t) = \alpha_{ij}(t)\beta_{ij}(t), \quad \epsilon_{ikj}^v(t) = \frac{\alpha_{ik}^v(t-1)\mathbf{P}_{itkj}P_j(\mathbf{y}_{it})\beta_{ij}^v(t)}{c_i(t)}. \quad (11)$$

Then, the $\Omega(\boldsymbol{\lambda}, \boldsymbol{\lambda}^v)$ can be written as the sum of three parts explicitly:

$$\Omega(\boldsymbol{\lambda}, \boldsymbol{\lambda}^v) = \text{constant} + h(\boldsymbol{\pi}) + h(\{\mathbf{B}_{kj}\}_{k,j=1}^J) - \frac{1}{2}h(\boldsymbol{\Psi}, \{\boldsymbol{\Lambda}_j\}_{j=1}^J, \{\boldsymbol{\mu}_j\}_{j=1}^J), \quad (12)$$

where $h(\boldsymbol{\pi})$ depends on the initial state distribution, $h(\{\mathbf{B}_{kj}\}_{k,j=1}^J)$ depends on the probability transition matrix, and $h(\boldsymbol{\Psi}, \{\boldsymbol{\Lambda}_j\}_{j=1}^J, \{\boldsymbol{\mu}_j\}_{j=1}^J)$ is a function of parameters $\boldsymbol{\Psi}$, $\boldsymbol{\Lambda}_j$ and $\boldsymbol{\mu}_j$. Explicit forms are provided in Section A.1 of the supplementary article.

3.2 Maximization (M-step)

Within each M-step, since $h(\boldsymbol{\Psi}, \{\boldsymbol{\Lambda}_j\}_{j=1}^J, \{\boldsymbol{\mu}_j\}_{j=1}^J)$, $h(\boldsymbol{\pi})$, and $h(\{\mathbf{B}_{kj}\}_{k,j=1}^J)$ do not share parameters, we maximize each of them separately. The estimator of $\boldsymbol{\pi}$, $\boldsymbol{\Lambda}_j$, $\boldsymbol{\mu}_j$, and $\boldsymbol{\Psi}$ can be easily derived by solving equations $h(\boldsymbol{\pi}) = 0$ and $h(\boldsymbol{\Psi}, \{\boldsymbol{\Lambda}_j\}_{j=1}^J, \{\boldsymbol{\mu}_j\}_{j=1}^J) = 0$ (see the explicit forms in Section A.2 in the supplementary article). Here, since we assume $\boldsymbol{\Psi}$ a diagonal matrix, we restrict all the off-diagonal entries of the estimator of $\boldsymbol{\Psi}$ to be 0. As for the rest of the parameters involved in the transition model, there is no explicit form of an MLE. Therefore, we use the one-step Newton-Raphson (NR) algorithm to update $\{\mathbf{B}_{kj}\}_{k,j=1}^J$ within each M-step.

First, considering the DT-EHMF, let \mathbf{S}_{kj} be the first-order partial derivative of $h(\{\mathbf{B}_{kj}\}_{k,j=1}^J)$ with respect to \mathbf{B}_{kj} and the (j, j') block entry of \mathbf{M}_k ($\mathbf{M}_k(j, j')$) to be the negative second-order partial derivative with respect to \mathbf{B}_{kj} and $\mathbf{B}_{kj'}$. Let \mathbf{S}_k and \mathbf{B}_k be defined similarly as $\mathbf{S}_k = (\mathbf{S}'_{k1}, \dots, \mathbf{S}'_{k,k-1}, \mathbf{S}'_{k,k+1}, \dots, \mathbf{S}'_{kJ})'$. Then \mathbf{B}_k is updated as

$\mathbf{B}_k^{v+1} = \mathbf{B}_k^v + \mathbf{M}_k^{-1} \mathbf{S}_k$. Alternatively, to ensure the stability of the algorithm and control the distance between \mathbf{B}_k^{v+1} and \mathbf{B}_k^v , we may update \mathbf{B}_k as $\mathbf{B}_k^{v+1} = \mathbf{B}_k^v + (\mathbf{M}_k + \mathbf{S}_k^T \mathbf{S}_k)^{-1} \mathbf{S}_k$.

Second, considering the CT-EHMF, though the likelihood function is in the same form as the DT-EHMF, the maximization step for CT-EHMF is more complicated as it involves operations of the matrix exponential. Let $\boldsymbol{\theta}$ be an ordered vector of all the transition model parameters, such that $\boldsymbol{\theta} = \text{vec}(\{\mathbf{B}'_{kj}, k \neq j\})$. Recalling the first derivative of the matrix exponential (Wilcox, 1967; Zhou et al., 2020) and using Theorem 1 in Van Loan (1978),

$$\frac{\partial}{\partial \theta_u} \exp(\mathbf{A}(\theta_u)) = \int_0^1 \exp(u\mathbf{A}(\theta_u)) \tilde{\mathbf{A}}(\theta_u) \exp((1-u)\mathbf{A}(\theta_u)) du = \exp(\mathbf{H})_{0:J, J:2J}, \quad (13)$$

where $\tilde{\mathbf{A}}(\theta_u) = (\tilde{A}_{ij}(\theta_u)) = (\frac{\partial A_{ij}(\theta_u)}{\partial \theta_u})$ and $\mathbf{H} = \begin{bmatrix} \mathbf{A}(\theta_u) & \tilde{\mathbf{A}}(\theta_u) \\ \mathbf{0} & \mathbf{A}(\theta_u) \end{bmatrix}$.

Denote $\frac{\partial \mathbf{P}_{kj}(\delta_{it})}{\partial \theta_u}$ as the (k, j) entry of the first derivative of $\mathbf{P}(\delta_{it})$ with respect to θ_u . Having the first derivative of $\exp(\delta_{it} * \mathbf{Q}) = \mathbf{P}(\delta_{it})$ with respect to each component of $\boldsymbol{\theta}$ calculated accordingly, a variant of NR, the Fisher scoring algorithm (FS) (Kalbfleisch and Lawless, 1985) can be directly implemented to update the parameter vector $\boldsymbol{\theta}$ to forbid the calculation of the second derivative of matrix exponential. Denote \mathbf{S}^* be the score function, and \mathbf{S}_u^* be the u^{th} entry of the score function \mathbf{S}^* . Then,

$$\mathbf{S}_u^*(\boldsymbol{\theta}) = \frac{\partial h(\{\mathbf{B}_{kj}\}_{k,j=1}^J)}{\partial \theta_u} = \sum_{i=1}^N \sum_{t=2}^{T_i} \sum_{j=1}^J \sum_{k=1}^J \frac{\epsilon_{ikj}^v(t)}{\mathbf{P}_{kj}(\delta_{it})} \frac{\partial \mathbf{P}_{kj}(\delta_{it})}{\partial \theta_u}. \quad (14)$$

Let \mathbf{M}^* be the negative Fisher information matrix. Its (u, v) entry \mathbf{M}_{uv}^* is in the form of:

$$\mathbf{M}_{uv}^*(\boldsymbol{\theta}) = \sum_{i=1}^N \sum_{t=2}^{T_i} \sum_{j=1}^J \sum_{k=1}^J \frac{\gamma_{ik}^v(t-1)}{\mathbf{P}_{kj}(\delta_{it})} \frac{\partial \mathbf{P}_{kj}(\delta_{it})}{\partial \theta_u} \frac{\partial \mathbf{P}_{kj}(\delta_{it})}{\partial \theta_v}. \quad (15)$$

After getting both the score function and the Fisher information matrix, parameters $\boldsymbol{\theta}$ can be updated as $\boldsymbol{\theta}^{v+1} = \boldsymbol{\theta}^v + \mathbf{M}^*(\boldsymbol{\theta}^v)^{-1} \mathbf{S}^*(\boldsymbol{\theta}^v)$. Similar to the DT-EHMF, a stabilized version is employed in practice with $\boldsymbol{\theta}^{v+1} = \boldsymbol{\theta}^v + \{\mathbf{M}^*(\boldsymbol{\theta}^v) + \mathbf{S}^*(\boldsymbol{\theta}^v)^T \mathbf{S}^*(\boldsymbol{\theta}^v)\}^{-1} \mathbf{S}^*(\boldsymbol{\theta}^v)$.

Furthermore, it is well-known that the choice of initial values for the EM algorithm and the NR/FS algorithm is essential for the algorithm's convergence and stability. Here, we make use of the Gaussian Mixture Model (GMM) and the FM to obtain good starting values. The complete iterative SEMIS algorithm is summarized in Algorithm 1.

Algorithm 1 Stabilized Expectation-Maximization Algorithm with Initialization Strategies (SEMIS)

```

1: procedure SEMIS( $\{\mathbf{Y}_i\}, \{\mathbf{X}_i\}, K, J, \delta_1, \delta_2$ )
2:   estimate initial values  $\boldsymbol{\lambda}$  (GMM, FM)
3:    $\boldsymbol{\lambda}^v \leftarrow \boldsymbol{\lambda}; \Delta^1 \leftarrow \delta_1 + 1; \Delta^2 \leftarrow \delta_2 + 1$ 
4:   while  $\Delta^1 > \delta_1$  and  $\Delta^2 > \delta_2$  do
5:     compute  $\gamma_{ij}^v(t), \epsilon_{ikj}^v(t)$ 
6:     update  $h(\boldsymbol{\pi}), h(\{\mathbf{B}_{kj}\}),$  and  $h(\boldsymbol{\Psi}, \{\boldsymbol{\Lambda}_j\}, \{\boldsymbol{\mu}_j\})$ 
7:     update  $\{\boldsymbol{\mu}_j\}, \{\boldsymbol{\Lambda}_j\}, \boldsymbol{\Psi}, \boldsymbol{\pi}$  by optimizing  $h(\boldsymbol{\pi}), h(\boldsymbol{\Psi}, \{\boldsymbol{\Lambda}_j\}, \{\boldsymbol{\mu}_j\})$ 
8:     update  $\{\mathbf{B}_{kj}\}$  based on  $h(\{\mathbf{B}_{kj}\})$  using stabilized NR/FS
9:      $\Delta^1 \leftarrow |\log P(\{\mathbf{Y}_i\}|\boldsymbol{\lambda}) - \log P(\{\mathbf{Y}_i\}|\boldsymbol{\lambda}^v)|$   $\triangleright$  absolute difference in log-likelihood
10:     $\Delta^2 \leftarrow \frac{\sum_l |\lambda_l^r - \lambda_l^v|}{r}$   $\triangleright$  average absolute difference in free parameters
11:     $\boldsymbol{\lambda}^v \leftarrow \boldsymbol{\lambda}$ 
12:   end while
13:   return  $\boldsymbol{\lambda}$  and  $\{w_{it}\} = \{\argmax_j(\gamma_{ij}(t))\}$ 
14: end procedure

```

4 Simulation Study

This section conducts a simulation study to evaluate the proposed methods on synthetic data generated randomly but resembling the AURORA data. The simulations are under similar settings as the AURORA data with respect to the sample size (N), number of observations per subject (T_i), number of response variables (p), and the number of covariates (d) in the transition model. Specifically, the synthetic data is randomly generated with

$N=200$, $p=23$, and $d=3$. T_i is specified differently for different models. See Section C in the supplementary article for the complete process of generating the synthetic data and the true values of the unknown parameters. In the following, subsection 4.1 evaluates the reliability of the proposed model by comparing the empirical results of parameter estimates and the true parameter values, and subsection 4.2 explores the performance of information criteria in model selection.

4.1 Simulation 1

To validate the estimation procedure, we implement the proposed SEMIS algorithm, assuming both J and K are known in advance. With the true J and true K , the pilot study showed that the proposed approach could efficiently choose initial values near the true parameter values, resulting in a fast convergence with no stabilization issue for both the CT-EHMF and the DT-EHMF. Therefore, for simplicity and computational efficiency, for each iteration, we update the parameters in the transition model using the standard one-step NR/FS algorithm without stabilization. Furthermore, based on the pilot study, we set the maximum iterations to 100 for each replication. The accuracy and reliability of the parameter estimates are then evaluated from two perspectives: i) accuracy of each parameter estimate and ii) misclassification rate (C_{mis}).

The accuracy of $\boldsymbol{\pi}$, $\boldsymbol{\mu}$, $\boldsymbol{\Lambda}$, and $\boldsymbol{\Psi}$ is calculated as the average absolute difference (AAD) between parameter estimates and true values. Mathematically, the AAD of a parameter matrix \boldsymbol{o} is

$$AAD(\boldsymbol{o}) = \frac{\sum_{i=1}^r |\hat{\boldsymbol{o}}_i - \boldsymbol{o}_i|}{r}, \quad (16)$$

where \boldsymbol{o}_i is a single entry in the matrix \boldsymbol{o} and r is the total number of free parameters in the parameter matrix \boldsymbol{o} . The mean of AADs (standard errors in the parentheses) aggregated

Table 1: Performance of Parameter Estimates

Parameter	π	μ	Λ	Ψ	C_{mis}
DT-EHMFMM	.027(.014)	.040(.005)	.037(.002)	.030(.005)	.0023(.0010)
CT-EHMFMM	.026(.013)	.015(.002)	.014(.001)	.011(.002)	.0024(.0005)

Table 2: Performance of Parameter Estimates in Transition Model

	DT-EHMFMM			CT-EHMFMM		
	B_{ij0}	B_{ij1}	B_{ij2}	B_{ij0}	B_{ij1}	B_{ij2}
B_{12}	-.050(.495)	-.067(.475)	-.006(.845)	.014(.142)	.017(.150)	-.080(.219)
B_{13}	-.024(.460)	.032(.408)	-.065(.700)	-.021(.126)	.010(.125)	.016(.182)
B_{21}	-.113(.483)	-.028(.409)	.104(.686)	-.018(.147)	-.004(.139)	.014(.214)
B_{23}	-.016(.453)	-.020(.426)	.050(.719)	-.003(.112)	.004(.097)	.005(.200)
B_{31}	-.037(.404)	-.055(.478)	-.007(.614)	.003(.112)	.002(.107)	-.006(.192)
B_{32}	-.013(.372)	-.016(.282)	.003(.561)	.006(.131)	-.032(.091)	.028(.232)

over 100 random seeds are presented in Table 1. For both the CT-EHMFMM and the DT-EHMFMM, the means of ADD of all parameter matrices are sufficiently closed to 0 with small standard error, implying a good parameter recovery.

For parameters in the transition model, the mean bias (standard error in the parenthesis) of each parameter is presented to evaluate the estimation accuracy in Table 2. For both CT-EHMFMM and DT-EHMFMM, the mean bias of each parameter in the transition model is closed to 0. However, the standard errors for each parameter estimate in the transition model of CT-EHMFMM are much smaller than that of DT-EHMFMM, which is mainly because of the unbalanced panel length T_i . While each subject under the setting of DT-EHMFMM has only ten observations, an individual has at least 50 observations under the setting of CT-EHMFMM. Additional simulations showed that T_i is one of the major factors that will affect the parameter estimation, which will be illustrated later.

In Table 1, the last column included the mean (standard deviation) of the misclassification rate, which is calculated as the number of incorrect classifications divided by the total number of observations. On average, only .24%(.0005) of observations are incorrectly classi-

fied under the CT-EHMFm settings, and .22%(.0010) of estimated classification is incorrect under the DT-HMFm settings. Therefore the SEMIS algorithm with either CT-EHMFm or DT-EHMFm did a good job at estimating latent states under current settings.

Intuitively, the performance of parameter estimates will be affected by different factors, including sample size, the number of measurements for each individual, size of J and K , size of common variance Ψ , distinctions in μ_j and Λ_j between states, and the transition frequency. With additional simulations for both DT-EHMFm and CT-EHMFm, it turns out that the estimation performance of μ , Λ , Ψ , B , and misclassification rate are improved as (i) the common variances decrease, or (ii) the difference in μ_j and Λ_j between states increase, or (iii) J decreases, or (iv) sample size (N)/or the panel length (T_i) increase. While either increasing the size of K or using a B inducing infrequent transitions does not have a strong effect on the estimations of most parameters, they enhance the precision of transition probability estimation, which results in a decrease in misclassification rate. The estimation of π is improved only by increasing sample size (N) or the state distinctions of μ . The details are reported in Section D of the supplementary article.

4.2 Simulation 2

For model selection, information criteria such as Akaike information criteria (AIC) and Bayesian information criteria (BIC) have been widely used. In this study, we investigate whether the AIC or BIC is a reliable source for determining the number of latent states and the numbers of factors at each state simultaneously. We use the same set of 100 generated datasets as before, but this time we implement the proposed methods with a different set of (J, K) . Let $J = \{2, 3, 4\}$ and $K = \{2, 3, 4\}$. We consider all the possible combinations of J and K , which are nine candidate models in total. We apply the method with all nine

Table 3: Performance BIC/AIC in Model Selection

	J	K	Percentage (DTE)	Percentage (CTE)
AIC	3	3	94%	100%
	4	3	6%	-
BIC	3	3	100%	100%

models to estimate the generated data for each replicate, respectively.

Different from fitting the data with true J and true K , there is no sufficient evidence to show that the chosen initial values are close to their maximum likelihood estimators (MLE). To avoid possible issues, including wild oscillation and nonconvergence as a result of the lack of stability of the Newton-Raphson algorithm with initial values far from the MLE, we keep the stabilization step in the SEMIS algorithm.

Table 3 reports the results based on 100 replications, indicating that BIC has a better performance on model selection than AIC. While AIC recommends a model with true J and true K only 94% of replicates in the simulation study for the DT-EHMF, BIC recommends accurately all the time. Simulation studies considering the CT-EHMF demonstrate that both AIC and BIC recommend the model with true J and K 100% of the time. Therefore, in the real case study, we use BIC as the criteria for model selection.

In summary, the sample size and the number of observations per individual of the processed AURORA data will provide reasonable parameter estimation and BIC-based model selection results.

5 Analysis of the AURORA Data

Because mobile device data is collected irregularly both within and between subjects in nature, we apply the more general method CT-EHMF to the smartwatch data from

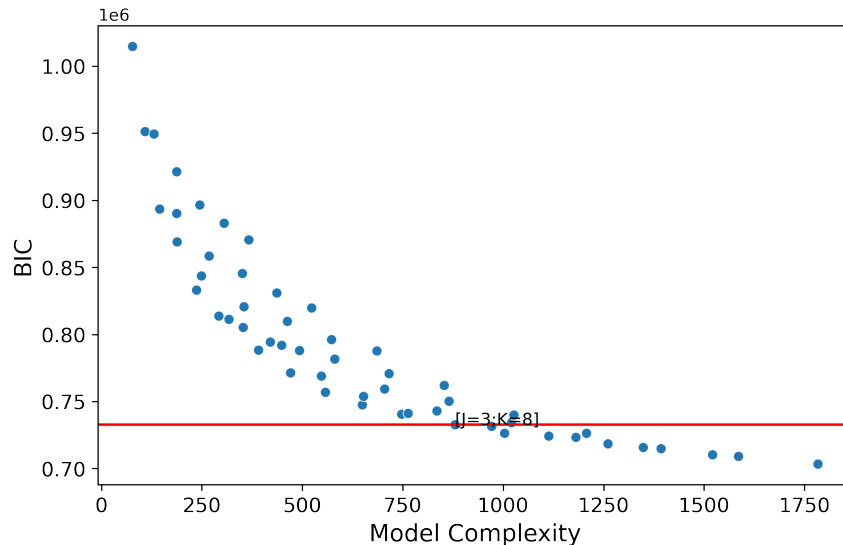


Figure 1: Plot of BIC versus the Model Complexity

the AURORA study. We consider a set of 54 candidate models ($J = \{1, 2, \dots, 6\}$; $K = \{1, 2, \dots, 9\}$). We implement the SEMIS algorithm with multiple random seeds for each candidate model and select the one with the maximum likelihood among all fitted models. In Figure 1, the BIC of each candidate model is displayed against the model complexity, which is the total number of free parameters in the model. Based on the BIC, a model with three states ($J = 3$) and eight factors per state ($K = 8$) is recommended. In the following, we concentrated on the interpretation of parameter estimates and biological findings from three perspectives: i) interpretation of three estimated states, ii) relationship between transition probability and age/gender, and iii) common structure of loading matrix.

5.1 Interpretation of Hidden States

To explore the biological difference between different states, we focus on the selected features. In Figure 2, scaled² sample means for each feature under different states are plotted along with their corresponding 95% confidence interval (CI). Further, based on the results

²Features are scaled to be in the range of $[0, 1]$, except for the NNskew.q3 whose range is $[-1, 1]$

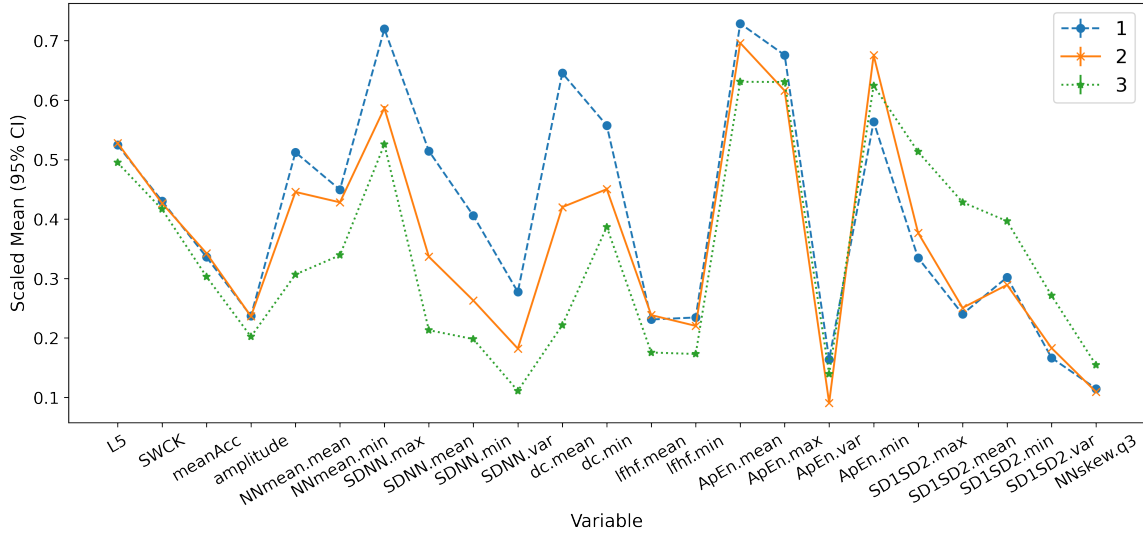


Figure 2: Relative Sample Mean for Features in Each Estimated States

of pairwise Tukey tests, the difference between states in almost all features is significant. However, for amplitude, SWCK, L5, and NNskew.q3, the difference between state 1 and state 2 are not statistically significant.

Overall, features related to average heart rate (NNmean related features), heart rate variability (SDNN related features), and the deceleration capacity of the heart (dc related features) are very different among the three latent states, with their values decreasing from state 1 to state 2, and then to state 3. Previous research suggests that lower heart rate variability and deceleration capacity are associated with a higher mortality rate (Kleiger et al., 2005; Kantelhardt et al., 2007). Furthermore, for activity features, state 1 and 2 have similar but higher means as compared with state 3, indicating that participants in state 1 and 2 have more daily activities and are healthier than state 3.

Among all the features related to the randomness or unpredictability of heart rate (lfhf, ApEn, and SD1SD2), state 3 has significantly higher values for SD1SD2 related features but lower values for lfhf related features than state 1 and state 2, which suggests opposite interpretations. However, previous studies suggest that the correspondence of these features

with the psychological and physiological state is not unique (von Rosenberg et al., 2017).

To confirm the validity of the three states, we further compare their differences regarding self-report symptoms collected from a flash survey (details are provided in Section F of the supplementary article). Based on the RDoC framework, ten latent constructs associated with APNS were developed using flash survey items selected by domain experts: Pain, Loss, Sleep Discontinuity, Nightmare, Somatic Symptoms, Mental Fatigue, Avoidance, Re-experience, and Anxious. Keeping only observations for each individual whose estimated states are known on the same day that they submit their survey responses, we summarized the flash survey data with means and 95% CI in Figure 3. While 0 stands for the least severe, 1 stands for the most severe.

Overall, for all ten symptoms constructs, state 1 has the lowest level of severity, and state 3 has the highest level of severity. Based on the Tukey tests, while states 1 and 2 are not statistically different on hyperarousal, re-experience, anxiety, and somatic symptoms, they are significantly different from state 1 on these constructs. Differences in the nightmare and sleep discontinuity between state 3 and state 2 are not significant but statistically more severe than state 1. For mental fatigue and depression, only the difference between state 1 and state 3 is statistically significant.

To investigate the pattern of the co-occurring symptoms under each hidden state, we focus on the observations in the first week. For each estimated state, we calculate the correlation between all ten symptoms. In the relative health state (state 1), a high degree of correlation exists between hyperarousal and anxiety, which implies that if a patient at state 1 experiences severe hyperarousal symptoms, it is highly likely that he or she may also suffer from severe anxiety symptoms. In other words, hyperarousal and anxiety are likely to co-occur among patients in state 1. A patient in state 2 can be expected to only

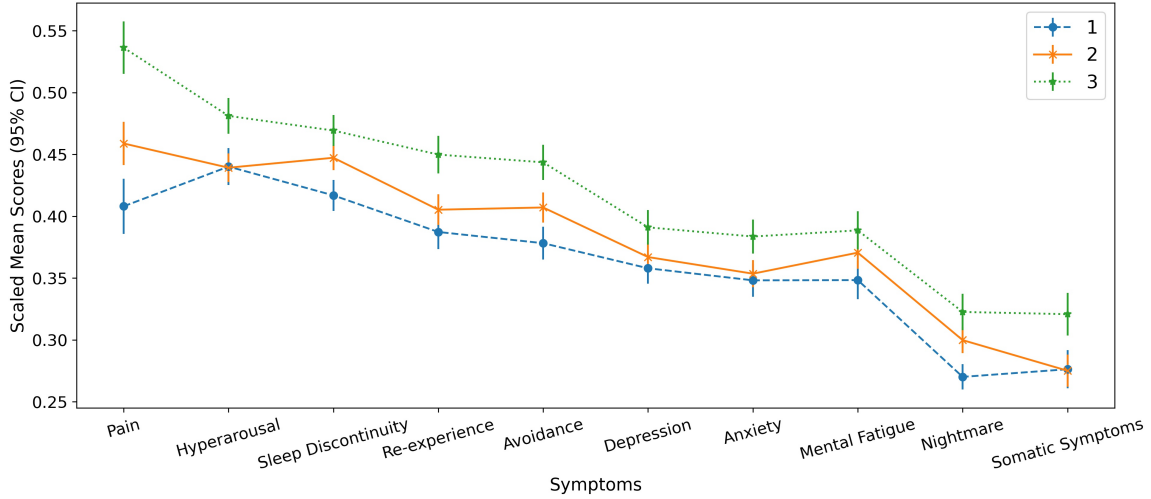


Figure 3: Sample Mean and Standard Deviation for Each Symptom in Each State

suffer from one symptom since none pair of the symptoms is highly correlated. Symptoms such as depression, hyperarousal, anxiousness, and re-experience are more likely to co-occur among patients with more severe disorders (state 3).

In summary, both the flash survey data and the AURORA data (HRV, Activity) demonstrate the consistent characteristics of three estimated hidden states. Among the three states, while state 1 is the healthiest, state 3 indicates the most severe APNS symptoms. While hyperarousal and anxiety tend to co-occur in state 1, symptoms including depression, hyperarousal, anxiousness, and re-experience are likely to co-occur in state 3. In state 2, symptoms are typically not co-occurring.

5.2 Transition Probability

Regarding the transition probabilities, here we mainly focus on the transition probabilities between states with time interval $\delta_{it} = 1$. We estimated the transition probabilities for both males and females within the sample range of age in Figure 4. While lines with circles depict the likelihood of remaining at the same station, lines with stars reflect the

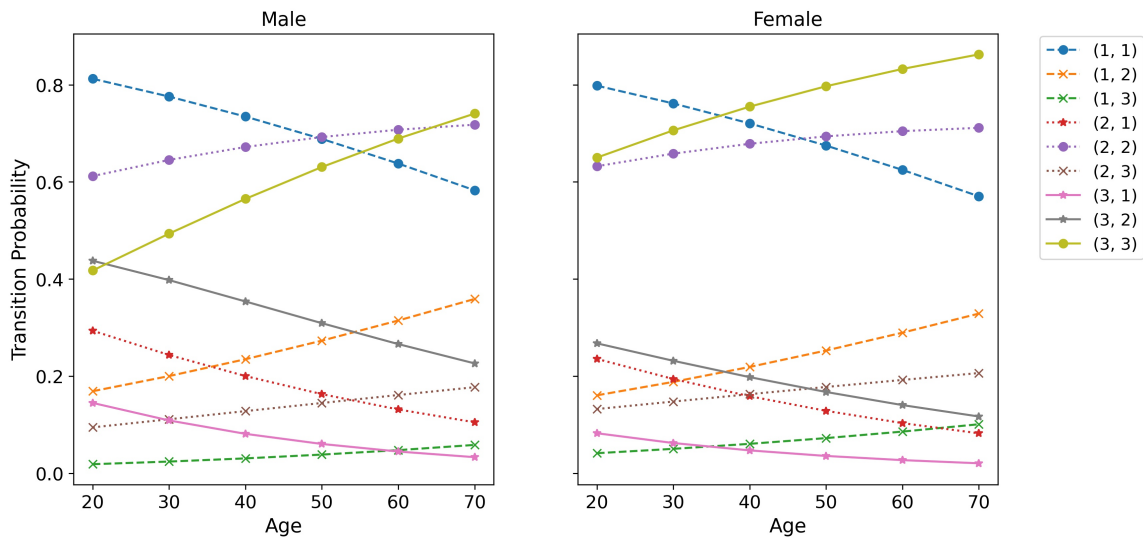


Figure 4: Estimated Transition Probability

probability of moving to a worse condition, and lines with “x” represent the possibility of a psychological condition improvement.

Overall, for both males and females, patients are more likely to stay in the same condition with infrequent state transitions, which is consistent with most existing literature. For the male group, the probability of staying at state 3 and state 2 rises with age, while the probability of staying at state 1 decreases with age. While the probability of psychological deterioration increases as age increases, the probability of psychological state improvement decreases as age increases. The tendency of the female group is similar to that of the male group, except that the probability of staying at the worst state (state 3) is much higher in the female group than in the male group.

The transition between state 1 and state 3 is the least possible. While the probability of transforming from state 3 to state 1 approaches 0 as age increases, the likelihood of the opposite transition approaches 0 as age decreases.

In summary, based on the analysis of the AURORA data, older patients are more likely to transit to a worse psychological state. Moreover, it becomes much harder to get

psychological improvement as age increases.

5.3 Factor Loading Structure

Finally, we are interested in the structure of the factor loading matrix that explains the correlations of observed features in each state. To facilitate the interpretation, the estimated loading matrix listed in Section E of the supplementary article is rotated by the promax rotation (Hendrickson and White, 1964; Browne, 2001), and then standardized by the estimated standard deviation of each variable ($\Lambda_j \Lambda_j' + \Psi$). Factor loadings with absolute values greater than .4 are bolded.

Overall, factor loading matrices among the three states share some similarities but also have some differences, implying heterogeneous covariance structures among different states. For all states, factor 0 is defined by heart rate variability and irregularity-related features. While the structure of factor 0 in Λ_2 and Λ_3 are the same, which is defined by SDDN-, dc- and ApEN-related features, only SDNN, and ApEn contribute to factor 0 in Λ_1 and dc-related features themselves contribute to the factor 7 in Λ_1 alone. Similarly, components of factor 2 are the same in state 2 and state 3, including lfhf and SD1SD2 related features. However, factor 2 in state 1 includes two additional SD1SD2 statistics which define the factor 5 in both state 2 and state 3.

Though factor 1 is defined by ApEn-related statistics for all states, the weighting of each statistic is different across states. Factor 3 is positively correlated to the mean heart rate (NNmean) and negatively correlated to the skewness of heart rate (NNskew). Factor 4 summarizes activity features, which shows a negative correlation between average activities (i.e., meanAcc, amplitude, and L5) and the number of transitions between wake and sleep (SWCK), suggesting that participants who have more activities during the daytime tend

to sleep better during the night. Factor 6 is solely defined by the summary statistics of SDNN.

In summary, while the factor loading matrix does not differ a lot between states, state distinction in means contributes the most to help distinguish different states.

6 Conclusions and Discussion

This paper investigates the unique challenges of analyzing longitudinal mobile health data, including high dimensionality and irregular measurements. We address these issues with two HMM-based models, DT-EHMFMM and CT-EHMFMM, for multivariate longitudinal data collected regularly and irregularly, respectively. In addition, we developed a SEMIS algorithm for maximum likelihood estimation, the performance of which is supported by a detailed simulation study. Finally, we analyzed the AURORA data and identified biological findings consistent with previous research, implying a great potential of the mobile health data for mental health research.

The proposed methods can be extended in several directions. First, it is easy to notice that most of the estimated factor loading matrix entries are closed to 0, indicating a sparse factor loading matrix. Different types of rotations are often applied to make the factor loading matrix easy to interpret. After that, factor loadings below certain cutoffs (0.4 or 0.7) are set to 0. However, the choice of cutoffs is subjective to some extent. The sparse exploratory factor loading analysis (Xie et al., 2010; Chen and Huang, 2012) provides a way to automatically set the loading entries of redundant variables to 0, which improves the interpretability of the loading matrix without the dependence on an arbitrary threshold. Therefore, a valuable extension for our current work is to incorporate sparse regularization into the factor loading matrix.

Furthermore, for real data analysis, a large number of baseline covariates are often collected. However, we do not have prior knowledge about which covariates might affect the transition probability. As a result, introducing regularization to the transition model to help variable selection is very useful.

Third, according to domain knowledge, mental health is extremely diverse. One strong assumption of the HMM is the independence between \mathbf{Y}_{it} given the hidden states. Intuitively, a violation of this assumption is highly possible, given the existence of autocorrelation between observations on the same subject. In other words, although features recorded bring much information to help determine the hidden state, there is heterogeneity even conditional on these features. Therefore, adding a random effect to the current model is a natural extension to account for the inter-patient heterogeneity (Altman, 2007; Song et al., 2017).

Finally, previous studies related to HRV are often conducted in a well-controlled lab environment, and all available tools used to derive HRV features are based on resting-state heart rate. However, heart rate data collected from a real-world open environment will introduce much additional noise. For example, it is reasonable to expect that HRV features corresponding to different activity states (e.g., exercise and resting) are very different. Noticing that there is no tool available to extract HRV features corresponding to different states, we believe developing a preprocessed pipeline for simultaneously processing heart rate and activity data to derive such HRV features would be worthwhile.

References

- Albert, A. (1962). Estimating the infinitesimal generator of a continuous time, finite state markov process. *The Annals of Mathematical Statistics*, pages 727–753.
- Altman, R. M. (2007). Mixed hidden markov models: an extension of the hidden markov model to the longitudinal data setting. *Journal of the American Statistical Association*, 102(477):201–210.
- Amoros, R., King, R., Toyoda, H., Kumada, T., Johnson, P. J., and Bird, T. G. (2019). A continuous-time hidden markov model for cancer surveillance using serum biomarkers with application to hepatocellular carcinoma. *Metron*, 77(2):67–86.
- Baum, L. E. and Petrie, T. (1966). Statistical Inference for Probabilistic Functions of Finite State Markov Chains. *The Annals of Mathematical Statistics*, 37(6):1554–1563. Publisher: Institute of Mathematical Statistics.
- Borazio, M., Berlin, E., Kücüküydiz, N., Scholl, P., and Van Laerhoven, K. (2014). Towards benchmarked sleep detection with wrist-worn sensing units. In *2014 IEEE International Conference on Healthcare Informatics*, pages 125–134. IEEE.
- Browne, M. W. (2001). An overview of analytic rotation in exploratory factor analysis. *Multivariate behavioral research*, 36(1):111–150.
- Cappé, O., Moulines, E., and Rydén, T. (2006). *Inference in hidden Markov models*. Springer Science & Business Media.
- Chen, L. and Huang, J. Z. (2012). Sparse reduced-rank regression for simultaneous dimension reduction and variable selection. *Journal of the American Statistical Association*, 107(500):1533–1545.

- Cole, R. J., Kripke, D. F., Gruen, W., Mullaney, D. J., and Gillin, J. C. (1992). Automatic sleep/wake identification from wrist activity. *Sleep*, 15(5):461–469.
- Cook, R. J., Kalbfleisch, J. D., and Yi, G. Y. (2002). A generalized mover–stayer model for panel data. *Biostatistics*, 3(3):407–420.
- Cornelissen, G. (2014). Cosinor-based rhythmometry. *Theoretical Biology and Medical Modelling*, 11(1):1–24.
- Cox, D. R. and Miller, H. D. (2017). *The theory of stochastic processes*. Routledge.
- Habtemichael, T. G., Goshu, A. T., and Buta, G. B. (2018). Missclassification of hiv disease stages with continuous time hidden markov models. *Journal of Advances in Medicine and Medical Research*, pages 1–15.
- Hartmann, R., Schmidt, F. M., Sander, C., and Hegerl, U. (2019). Heart rate variability as indicator of clinical state in depression. *Frontiers in psychiatry*, 9:735.
- Hendrickson, A. E. and White, P. O. (1964). Promax: A quick method for rotation to oblique simple structure. *British journal of statistical psychology*, 17(1):65–70.
- Insel, T. R. (2017). Digital phenotyping: technology for a new science of behavior. *Jama*, 318(13):1215–1216.
- Jung, W., Jang, K.-I., and Lee, S.-H. (2019). Heart and brain interaction of psychiatric illness: a review focused on heart rate variability, cognitive function, and quantitative electroencephalography. *Clinical Psychopharmacology and Neuroscience*, 17(4):459.
- Kalbfleisch, J. and Lawless, J. F. (1985). The analysis of panel data under a markov assumption. *Journal of the american statistical association*, 80(392):863–871.

- Kantelhardt, J. W., Bauer, A., Schumann, A. Y., Barthel, P., Schneider, R., Malik, M., and Schmidt, G. (2007). Phase-rectified signal averaging for the detection of quasi-periodicities and the prediction of cardiovascular risk. *Chaos: An Interdisciplinary Journal of Nonlinear Science*, 17(1):015112.
- Kim, J.-O. and Mueller, C. W. (1978). *Factor analysis: Statistical methods and practical issues*, volume 14. sage.
- Kleiger, R. E., Stein, P. K., and Bigger Jr, J. T. (2005). Heart rate variability: measurement and clinical utility. *Annals of Noninvasive Electrocardiology*, 10(1):88–101.
- Liu, X. and Chen, R. (2016). Regime-Switching Factor Models for High-Dimensional Time Series. *Statistica Sinica*, 26(4):1427–1451.
- Liu, Y.-Y., Li, S., Li, F., Song, L., and Rehg, J. M. (2015). Efficient learning of continuous-time hidden markov models for disease progression. *Advances in neural information processing systems*, 28:3599.
- Madadi, M. (2019). A hidden markov factor analysis framework for seizure detection in epilepsy patients.
- Marquand, A. F., Wolfers, T., Mennes, M., Buitelaar, J., and Beckmann, C. F. (2016). Beyond lumping and splitting: a review of computational approaches for stratifying psychiatric disorders. *Biological psychiatry: cognitive neuroscience and neuroimaging*, 1(5):433–447.
- Maruotti, A., Bulla, J., Lagona, F., Picone, M., and Martella, F. (2017). Dynamic mixtures of factor analyzers to characterize multivariate air pollutant exposures. *The Annals of Applied Statistics*, 11(3):1617–1648.

- McLean, S. A., Ressler, K., Koenen, K. C., Neylan, T., Germine, L., Jovanovic, T., Clifford, G. D., Zeng, D., An, X., Linnstaedt, S., et al. (2020). The aurora study: a longitudinal, multimodal library of brain biology and function after traumatic stress exposure. *Molecular psychiatry*, 25(2):283–296.
- Osborne, J. (2010). Improving your data transformations: Applying the box-cox transformation. *Practical Assessment, Research, and Evaluation*, 15(1):12.
- Rabiner, L. R. (1989). A tutorial on hidden markov models and selected applications in speech recognition. *Proceedings of the IEEE*, 77(2):257–286.
- Rasmussen, C. E. (2003). Gaussian processes in machine learning. In *Summer school on machine learning*, pages 63–71. Springer.
- Ross, S. M., Kelly, J. J., Sullivan, R. J., Perry, W. J., Mercer, D., Davis, R. M., Washburn, T. D., Sager, E. V., Boyce, J. B., and Bristow, V. L. (1996). *Stochastic processes*, volume 2. Wiley New York.
- Rosti, A. I. and Gales, M. (2004). Factor analysed hidden markov models for speech recognition. *Computer Speech & Language*, 18(2):181–200.
- Rosti, A. I. and Gales, M. J. (2002). Factor analysed hidden markov models. In *2002 IEEE International Conference on Acoustics, Speech, and Signal Processing*, volume 1, pages I–949. IEEE.
- Shaffer, F. and Ginsberg, J. P. (2017). An overview of heart rate variability metrics and norms. *Frontiers in public health*, 5:258.
- Song, X., Xia, Y., and Zhu, H. (2017). Hidden Markov latent variable models with multivariate longitudinal data. *Biometrics*, 73(1):313–323.

- Titman, A. C. (2011). Flexible nonhomogeneous markov models for panel observed data. *Biometrics*, 67(3):780–787.
- Van Loan, C. (1978). Computing integrals involving the matrix exponential. *IEEE transactions on automatic control*, 23(3):395–404.
- Van Someren, E. J., Swaab, D. F., Colenda, C. C., Cohen, W., McCall, W. V., and Rosenquist, P. B. (1999). Bright light therapy: improved sensitivity to its effects on rest-activity rhythms in alzheimer patients by application of nonparametric methods. *Chronobiology international*, 16(4):505–518.
- Vermunt, J. K., Langeheine, R., and Bockenholt, U. (1999). Discrete-time discrete-state latent markov models with time-constant and time-varying covariates. *Journal of Educational and Behavioral Statistics*, 24(2):179–207.
- von Rosenberg, W., Chanwimalueang, T., Adjei, T., Jaffer, U., Goverdovsky, V., and Mandic, D. P. (2017). Resolving ambiguities in the lf/hf ratio: Lf-hf scatter plots for the categorization of mental and physical stress from hrv. *Frontiers in physiology*, 8:360.
- Wilcox, R. M. (1967). Exponential operators and parameter differentiation in quantum physics. *Journal of Mathematical Physics*, 8(4):962–982.
- Xie, B., Pan, W., and Shen, X. (2010). Penalized mixtures of factor analyzers with application to clustering high-dimensional microarray data. *Bioinformatics*, 26(4):501–508.
- Zhou, J., Song, X., and Sun, L. (2020). Continuous time hidden markov model for longitudinal data. *Journal of Multivariate Analysis*, 179:104646.

Supplement to “Exploratory Hidden Markov Factor Models for Longitudinal Mobile Health Data: Application to Adverse Posttraumatic Neuropsychiatric Sequelae”

Lin Ge, Xinming An, Donglin Zeng,

Samuel McLean, Ronald Kessler, and Rui Song

This supplementary article is organized as follows. In Section A, we show the explicit forms of the components in the $\Omega(\lambda, \lambda^v)$ and the explicit forms of the MLE of $\boldsymbol{\pi}$, Λ , and $\boldsymbol{\Psi}$. Section B illustrates how we pre-process the data for analysis, while Section C contains the data generation process for the simulation study. Additional simulation results are given in Section D, and additional real analysis results are presented in Section E. Finally, in Section F, information about the flash survey data we used for the real analysis is provided.

A More Technical Details

In this section, we show the explicit forms of the components in the $\Omega(\lambda, \lambda^v)$ and the explicit forms of the MLE of $\boldsymbol{\pi}$, Λ , and $\boldsymbol{\Psi}$.

A.1 Supplement for E-step

Denote $\widetilde{\Lambda}_j = (\Lambda_j, \boldsymbol{\mu}_j) \in \mathcal{R}^{p \times (K+1)}$ and $\widetilde{\mathbf{z}}_{it} = (\mathbf{z}_{it}^T, 1)^T \in \mathcal{R}^{(K+1)}$. Each of the three parts has an explicit form as follows:

$$h(\boldsymbol{\pi}) = \sum_{i=1}^N \sum_{j=1}^J \gamma_{ij}^v(1) \log(\pi_j), \quad (\text{S.1})$$

$$h(\{\mathbf{B}_{kj}\}_{k,j=1}^J) = \sum_{i=1}^N \sum_{t=2}^{T_i} \sum_{j,k=1}^J \epsilon_{ikj}^v(t) \log(\mathbf{P}_{itkj}), \quad (\text{S.2})$$

$$\begin{aligned} h(\Psi, \{\Lambda_j\}_{j=1}^J, \{\mu_j\}_{j=1}^J) &= \sum_{i=1}^N \sum_{t=1}^{T_i} \sum_{j=1}^J \gamma_{ij}^v(t) \log|\Psi| \\ &\quad + \gamma_{ij}^v(t) \mathbf{y}'_{it} \Psi^{-1} \mathbf{y}_{it} - 2\gamma_{ij}^v(t) \mathbf{y}'_{it} \Psi^{-1} \widetilde{\Lambda}_j E_{\lambda^v}(\widetilde{\mathbf{z}}_{it} | \mathbf{y}_{it}, w_{it}) \\ &\quad + \gamma_{ij}^v(t) \text{tr}(\widetilde{\Lambda}_j' \Psi^{-1} \widetilde{\Lambda}_j E_{\lambda^v}(\widetilde{\mathbf{z}}_{it} \widetilde{\mathbf{z}}_{it}' | \mathbf{y}_{it}, w_{it})). \end{aligned} \quad (\text{S.3})$$

Note that, in the discrete-time case, the $\log(\mathbf{P}_{itkj})$ in the equation (S.2) can be further expressed as $\mathbf{x}_{it}^T \mathbf{B}_{kj} - \log(\sum_{l=1}^J e^{\mathbf{x}_{it}^T \mathbf{B}_{kl}})$. Using the Woodbury matrix identity (Rasmussen, 2003), let $\mathbf{M}_j^v = (I + \Lambda_j^{v'} \Psi^{v-1} \Lambda_j^v)^{-1}$, two expectation terms in $h(\Psi, \{\Lambda_j\}_{j=1}^J, \{\mu_j\}_{j=1}^J)$ has the explicit form as:

$$E_{\lambda^v}(\widetilde{\mathbf{z}}_{it} | \mathbf{y}_{it}, w_{it}) = \begin{bmatrix} \mathbf{M}_j^v \Lambda_j^{v'} \Psi^{v-1} (\mathbf{y}_{it} - \mu_j^v) \\ 1 \end{bmatrix}, \quad (\text{S.4})$$

$$E_{\lambda^v}(\widetilde{\mathbf{z}}_{it} \widetilde{\mathbf{z}}_{it}' | \mathbf{y}_{it}, w_{it}) = \begin{bmatrix} \mathbf{M}_j^v + E_{\lambda^v}(\mathbf{z}_{it} | \mathbf{y}_{it}, w_{it}) E_{\lambda^v}(\mathbf{z}'_{it} | \mathbf{y}_{it}, w_{it}) & E_{\lambda^v}(\mathbf{z}_{it} | \mathbf{y}_{it}, w_{it}) \\ E_{\lambda^v}(\mathbf{z}'_{it} | \mathbf{y}_{it}, w_{it}) & 1 \end{bmatrix}. \quad (\text{S.5})$$

A.2 Supplement for M-step

Within each M-step, since $h(\boldsymbol{\pi})$, $h(\{\mathbf{B}_{kj}\}_{k,j=1}^J)$, and $h(\Psi, \{\Lambda_j\}_{j=1}^J, \{\mu_j\}_{j=1}^J)$ do not share parameters, we maximize each of them separately. By solving the first derivative of $h(\boldsymbol{\pi})$ equal to 0, the parameters related to the initial state distribution are estimated as follows:

$$\pi_j^{new} = \frac{\sum_{i=1}^N \gamma_{ij}^v(1)}{\sum_{i=1}^N \sum_{k=1}^J \gamma_{ik}^v(1)}. \quad (\text{S.6})$$

Similarly, the parameters used to characterize the conditional distribution of \mathbf{y}_{it} given w_{it} are estimated by setting the first derivative of $h(\Psi, \{\Lambda_j\}_{j=1}^J, \{\mu_j\}_{j=1}^J)$ equal to 0. Λ_j will be updated as follows:

$$\widetilde{\Lambda}_j^{new} = \left\{ \sum_{i=1}^N \sum_{t=1}^{T_i} \gamma_{ij}^v(t) \mathbf{y}_{it} E_{\lambda^v}(\widetilde{\mathbf{z}}_{it} | \mathbf{y}_{it}, w_{it})' \right\} \left\{ \sum_{i=1}^N \sum_{t=1}^{T_i} \gamma_{ij}^v(t) E_{\lambda^v}(\widetilde{\mathbf{z}}_{it} \widetilde{\mathbf{z}}_{it}' | \mathbf{y}_{it}, w_{it}) \right\}^{-1}. \quad (\text{S.7})$$

Simultaneously, we got the updated estimation of Ψ as the following.

$$\Psi^{new} = \frac{1}{\sum_{i=1}^N T_i} \text{diag} \left\{ \sum_{i=1}^N \sum_{t=1}^{T_i} \sum_{j=1}^J \gamma_{ij}^v(t) \{ \mathbf{y}_{it} - \widetilde{\Lambda}_j^{new} E_{\lambda^v}(\widetilde{\mathbf{z}}_{it}) \} \mathbf{y}_{it}' \right\}. \quad (\text{S.8})$$

Here, since we assume Ψ a diagonal matrix, we restrict all the off-diagonal entries of the estimator of Ψ to be 0.

B Data Preparation

In this paper, we consider a subset of the AURORA data by selecting patients involved in MVC before presenting to the ED to investigate the dynamic change in patients' mental health conditions in the 100 days following MVC exposure. We maintain only observations with no missing data and a positive wake percentage when looking at the activity data. In terms of heart rate data, each individual is anticipated to have 2880 records every day. In mobile health data, however, missing data is widespread. We keep only observations on days with more than 30% ($2880 * 0.3$) recordings to derive representative daily summary statistics.

Prior to fitting our model, we further use the Box-Cox transformation (Osborne, 2010) on each variable to reduce the skewness of the original data, delete extreme values, remove highly-correlated features, and scale the data by dividing the sample standard deviation

for each variable.

The final dataset we used included observations collected from 258 patients, each having a different number of total daily records ranging from 17 to 99. Note that observations in this dataset are irregularly sampled. Therefore, a subset of it, including only observations collected at $\{\text{day 2, day 12, } \dots, \text{day 82}\}$, is also of our interest. In the subset with systematic observations, 180 patients are included.

Based on domain knowledge, 23 variables are of our main interest. Four of them are derived from the activity data, while the remaining 19 are derived from the HRV data (i.e., meanAcc, amplitude, SWCK, L5, NNmean.min, NNmean.mean, NNskew.q3, SDNN.max, SDNN.min, SDNN.mean, SDNN.var, lfhf.min, lfhf.mean, dc.min, dc.mean, SD1SD2.max, SD1SD2.min, SD1SD2.mean, SD1SD2.var, ApEn.max, ApEn.min, ApEn.mean, ApEn.var). Besides, the transition model includes both age (range from 18-74) and gender (0-male, 1-female) to investigate the effect of age and gender on the transition probabilities.

C Synthetic Data Generation

To resemble the processed AURORA data allowing irregular measurements, in the test of CT-EHMF, T_i is an integer uniformly sampled from the interval $[50, 100]$ for each subject. Noticing that time intervals are needed for the CT-EHMF, after sampling T_i , we randomly selected T_i integers from the $\{1, \dots, 100\}$ without replacement. Then the ordered sequence of T_i integers is the sequence of the occasions (t) getting measurements, and the time interval δ_{it} is calculated accordingly. To closely replicate the processed AURORA data with only regular measurements, in the test of DT-EHMF, T_i fixed at 10 for all subjects.

Let the number of states J and the number of factors K both fixed at three. We first generated data related to the latent states. The initial state of each individual is inde-

pendently sampled from the multinomial distribution with initial probability $\boldsymbol{\pi} = (\frac{1}{3}, \frac{1}{3}, \frac{1}{3})$. With the initial states, each individual’s latent state trajectories are then sampled according to the transition probabilities \mathbf{P}_{it} or $\mathbf{P}_{it}(\delta_{it})$ with $\{\mathbf{B}_{kj}\}$ and $\mathbf{x}_{it}^T = (x_{it1}, x_{it2}, x_{it3})$. To replicate the AURORA data, we assume all the three covariates in the transition model are baseline features that are static across time. While $x_{it1} = 1$ for an intercept, x_{it2} is a binary variable sampled from $\{0, 1\}$ uniformly and independently and x_{it3} follows a uniform distribution between 0 and 1. Given the dynamic trajectories of states for each individual, suppose individual i is in the state j at time t , the vector of observation \mathbf{y}_{it} is then randomly drawn from a normal distribution with mean $\boldsymbol{\mu}_j$ and covariance $\boldsymbol{\Lambda}_j \boldsymbol{\Lambda}_j' + \boldsymbol{\Psi}$, where $\boldsymbol{\Psi}$ is assumed to be an identity matrix. The true values of the unknown parameters are summarized in Table S.1.

Table S.1: True Parameters

j	1	2	3
$\boldsymbol{\mu}_j$	$\begin{pmatrix} 15 * \mathbf{1}_2 \\ 10 * \mathbf{1}_3 \\ 5 * \mathbf{1}_6 \\ 0 * \mathbf{1}_{12} \end{pmatrix}$	$\begin{pmatrix} 17 * \mathbf{1}_2 \\ 12 * \mathbf{1}_3 \\ 7 * \mathbf{1}_6 \\ 2 * \mathbf{1}_{12} \end{pmatrix}$	$\begin{pmatrix} 19 * \mathbf{1}_2 \\ 14 * \mathbf{1}_3 \\ 9 * \mathbf{1}_6 \\ 4 * \mathbf{1}_{12} \end{pmatrix}$
$\boldsymbol{\Lambda}_j$	$\begin{pmatrix} 1 * \mathbf{1}_2 & 1 * \mathbf{1}_2 & 1 * \mathbf{1}_2 \\ .7 * \mathbf{1}_5 & 0 * \mathbf{1}_5 & 0 * \mathbf{1}_5 \\ 0 * \mathbf{1}_8 & .7 * \mathbf{1}_8 & 0 * \mathbf{1}_8 \\ 0 * \mathbf{1}_8 & 0 * \mathbf{1}_8 & .7 * \mathbf{1}_8 \end{pmatrix}$	$\begin{pmatrix} 0 * \mathbf{1}_2 & .7 * \mathbf{1}_2 & 0 * \mathbf{1}_2 \\ 1 * \mathbf{1}_2 & 1 * \mathbf{1}_2 & 1 * \mathbf{1}_2 \\ 0 * \mathbf{1}_3 & .7 * \mathbf{1}_3 & 0 * \mathbf{1}_3 \\ .7 * \mathbf{1}_8 & 0 * \mathbf{1}_8 & 0 * \mathbf{1}_8 \\ 0 * \mathbf{1}_8 & 0 * \mathbf{1}_8 & .7 * \mathbf{1}_8 \end{pmatrix}$	$\begin{pmatrix} 0 * \mathbf{1}_4 & 0 * \mathbf{1}_4 & .7 * \mathbf{1}_4 \\ 1 * \mathbf{1}_2 & 1 * \mathbf{1}_2 & 1 * \mathbf{1}_2 \\ 0 & 0 & .7 \\ 0 * \mathbf{1}_8 & .7 * \mathbf{1}_8 & 0 * \mathbf{1}_8 \\ .7 * \mathbf{1}_8 & 0 * \mathbf{1}_8 & 0 * \mathbf{1}_8 \end{pmatrix}$
\mathbf{B}_{1j}^T (DT)	/	$(-2.95 \quad -1 \quad .5)$	$(-2.95 \quad -.5 \quad .5)$
\mathbf{B}_{2j}^T (DT)	$(-2.95 \quad -.5 \quad .5)$	/	$(-2.95 \quad -.5 \quad .5)$
\mathbf{B}_{3j}^T (DT)	$(-2.95 \quad -.5 \quad .5)$	$(-2.95 \quad 1 \quad .5)$	/
\mathbf{B}_{1j}^T (CT)	/	$(-2.5 \quad 1 \quad -1)$	$(-2.5 \quad 1 \quad -1)$
\mathbf{B}_{2j}^T (CT)	$(-3 \quad 1 \quad -1)$	/	$(-2.5 \quad 1 \quad -1)$
\mathbf{B}_{3j}^T (CT)	$(-3 \quad 1 \quad -1)$	$(-3 \quad 1 \quad -1)$	/

D Additional Simulation Results

This section concludes all the results of additional simulation results reflecting how the estimation performance being affected by different factor, including sample size, number of

measurements for each individual, size of J and K , size of common variance Ψ , distinctions in μ_j and Λ_j between states, and the transition frequency.

First, we would like to illustrate different setups that we used in the simulation. The baseline setup is exactly the setups that we described in Section C. For each test, we keep all the setups the same as the baseline setups except for the factor tested. Specifically, in the baseline setup, the common variance is 1, the difference between μ_j 's is large, the difference between Λ_j 's is large, and the transition model induces infrequent transition (i.e, the probability remaining at the same state is at least .75).

For the test regarding the effect of common variance Ψ , we consider the common variance to be $.1\mathbf{I}$, $.5\mathbf{I}$ and $1\mathbf{I}$ (baseline). For the test regarding the effect of μ distinction, we define the medium difference and minor difference as the following:

Table S.2: μ with Medium Difference and Minor Difference

j	1	2	3
μ :medium diff	$\begin{pmatrix} 15 * \mathbf{1}_2 \\ 10 * \mathbf{1}_3 \\ 5 * \mathbf{1}_6 \\ 0 * \mathbf{1}_{12} \end{pmatrix}$	$\begin{pmatrix} 17 * \mathbf{1}_2 \\ 12 * \mathbf{1}_3 \\ 7 * \mathbf{1}_6 \\ 0 * \mathbf{1}_{12} \end{pmatrix}$	$\begin{pmatrix} 19 * \mathbf{1}_2 \\ 14 * \mathbf{1}_3 \\ 9 * \mathbf{1}_6 \\ 0 * \mathbf{1}_{12} \end{pmatrix}$
μ :minor diff	$\begin{pmatrix} 15 * \mathbf{1}_2 \\ 10 * \mathbf{1}_3 \\ 5 * \mathbf{1}_6 \\ 0 * \mathbf{1}_{12} \end{pmatrix}$	$\begin{pmatrix} 15.75 * \mathbf{1}_2 \\ 10.75 * \mathbf{1}_3 \\ 5 * \mathbf{1}_6 \\ 0 * \mathbf{1}_{12} \end{pmatrix}$	$\begin{pmatrix} 16.5 * \mathbf{1}_2 \\ 11.5 * \mathbf{1}_3 \\ 5 * \mathbf{1}_6 \\ 0 * \mathbf{1}_{12} \end{pmatrix}$

For the test regarding the effect of Λ distinction, we define the medium difference and minor difference as the following:

Table S.3: Λ with Medium Difference and Minor Difference

j	1	2	3
Λ : medium diff	$\begin{pmatrix} .3 & .3 & .3 \\ .7 * \mathbf{1}_6 & 0 * \mathbf{1}_6 & 0 * \mathbf{1}_6 \\ 0 * \mathbf{1}_8 & .7 * \mathbf{1}_8 & 0 * \mathbf{1}_8 \\ 0 * \mathbf{1}_8 & 0 * \mathbf{1}_8 & .7 * \mathbf{1}_8 \end{pmatrix}$	$\begin{pmatrix} .7 * \mathbf{1}_3 & 0 * \mathbf{1}_3 & 0 * \mathbf{1}_3 \\ .3 & .3 & .3 \\ .7 * \mathbf{1}_3 & 0 * \mathbf{1}_3 & 0 * \mathbf{1}_3 \\ 0 * \mathbf{1}_8 & .7 * \mathbf{1}_8 & 0 * \mathbf{1}_8 \\ 0 * \mathbf{1}_8 & 0 * \mathbf{1}_8 & .7 * \mathbf{1}_8 \end{pmatrix}$	$\begin{pmatrix} .7 * \mathbf{1}_5 & 0 * \mathbf{1}_5 & 0 * \mathbf{1}_5 \\ .3 & .3 & .3 \\ .7 & 0 & 0 \\ 0 * \mathbf{1}_8 & .7 * \mathbf{1}_8 & 0 * \mathbf{1}_8 \\ 0 * \mathbf{1}_8 & 0 * \mathbf{1}_8 & .7 * \mathbf{1}_8 \end{pmatrix}$
Λ : minor diff	$\begin{pmatrix} .05 & .05 & .05 \\ .7 * \mathbf{1}_6 & 0 * \mathbf{1}_6 & 0 * \mathbf{1}_6 \\ 0 * \mathbf{1}_8 & .7 * \mathbf{1}_8 & 0 * \mathbf{1}_8 \\ 0 * \mathbf{1}_8 & 0 * \mathbf{1}_8 & .7 * \mathbf{1}_8 \end{pmatrix}$	$\begin{pmatrix} .7 * \mathbf{1}_3 & 0 * \mathbf{1}_3 & 0 * \mathbf{1}_3 \\ .05 & .05 & .05 \\ .7 * \mathbf{1}_3 & 0 * \mathbf{1}_3 & 0 * \mathbf{1}_3 \\ 0 * \mathbf{1}_8 & .7 * \mathbf{1}_8 & 0 * \mathbf{1}_8 \\ 0 * \mathbf{1}_8 & 0 * \mathbf{1}_8 & .7 * \mathbf{1}_8 \end{pmatrix}$	$\begin{pmatrix} .7 * \mathbf{1}_5 & 0 * \mathbf{1}_5 & 0 * \mathbf{1}_5 \\ .05 & .05 & .05 \\ .7 & 0 & 0 \\ 0 * \mathbf{1}_8 & .7 * \mathbf{1}_8 & 0 * \mathbf{1}_8 \\ 0 * \mathbf{1}_8 & 0 * \mathbf{1}_8 & .7 * \mathbf{1}_8 \end{pmatrix}$

For the test regarding the effect of the transition probability, we define the frequent transition as the probability of staying at the same state with the probability less than .70.

The \mathbf{B} corresponding to the frequent transition probability is as the following:

Table S.4: \mathbf{B} with Frequent Transition

j	1	2	3
\mathbf{B}_{1j}^T (DT) : freq transit	/	(-1.5 -2 .75)	(-1.5 .75 .5)
\mathbf{B}_{2j}^T (DT) : freq transit	(-1.5 .75 1.25)	/	(-1.5 -1.5 .75)
\mathbf{B}_{3j}^T (DT) : freq transit	(-1.5 .75 .75)	(-1.5 -2 .75)	/
\mathbf{B}_{1j}^T (CT) : freq transit	/	(.5 1 -.5)	(.5 1 -.5)
\mathbf{B}_{2j}^T (CT) : freq transit	(-1 .5 1)	/	(-.25 1 -.5)
\mathbf{B}_{3j}^T (CT) : freq transit	(.5 .5 1)	(-.5 .5 1)	/

For tests regarding the effect of J and K , we simply adapt the baseline setups accordingly and not report it here. Table S.5 includes the results demonstrating the effect of different parameters and J/K under the DT-EHMFm settings, while Table S.7 includes results under the CT-EHMFm settings. Table S.6 and Table S.8 include the estimation results for different sample size (N) and different panel length (T_i) for DT-EHMFm and CT-EHMFm, respectively.

Table S.5: Performance of Parameter Estimates Affected by Parameters (DT-HMFm)

ADD	π	μ	Λ	Ψ	B	C_{mis}
$\Psi = 1 * I$.027(.014)	.040(.005)	.037(.002)	.030(.005)	.408 (.099)	.002(.001)
$\Psi = .5 * I$.027(.014)	.033(.005)	.027(.002)	.014(.002)	.407(.095)	.0003(.0004)
$\Psi = .1 * I$.027(.014)	.026(.006)	.018(.002)	.003(.001)	.407(.095)	.0000(.0000)
μ : large diff	.027(.014)	.040(.005)	.037(.002)	.030(.005)	.408 (.099)	.002(.001)
μ : medium diff	.027(.014)	.040(.005)	.038(.002)	.030(.005)	.426(.103)	.007(.002)
μ : minor diff	.034(.022)	.089(.056)	.098(.048)	.032(.008)	.714(.338)	.336(.290)
Λ : large diff	.027(.014)	.040(.005)	.037(.002)	.030(.005)	.408 (.099)	.002(.001)
Λ : medium diff	.027(.014)	.038(.004)	.037(.002)	.029(.005)	.422(.101)	.005(.002)
Λ : minor diff	.027(.014)	.038(.004)	.046(.002)	.030(.005)	.414(.098)	.004(.001)
B : infreq transit	.027(.014)	.040(.005)	.037(.002)	.030(.005)	.408 (.099)	.002(.001)
B : freq transit	.027(.014)	.041(.005)	.039(.002)	.031(.005)	.286 ^a (.080)	.005(.002)
$J = 2$.031(.023)	.032(.005)	.031(.002)	.029(.005)	.340 (.132)	.001(.001)
$J = 3$.027(.014)	.040(.005)	.037(.002)	.030(.005)	.408 (.099)	.002(.001)
$J = 4$.025(.010)	.046(.004)	.043(.002)	.030(.004)	.512(.094)	.003(.001)
$K = 2$.027(.014)	.040(.006)	.037(.002)	.029(.005)	.421 (.098)	.006(.002)
$K = 3$.027(.014)	.040(.005)	.037(.002)	.030(.005)	.408 (.099)	.002(.001)
$K = 5$.027(.014)	.041(.005)	.040(.002)	.034(.005)	.408(.095)	.0004(.0004)

^aNote that the ADD of the corresponding estimated transition probability matrix with frequent transit is .033(.012), while that with infrequent transit is .022(.009). Since for each individual, there are only 10 observations, frequent transition will definitely help estimating the transition model with more different observations. However, the estimated probability matrix might be affected differently.

Table S.6: Performance of Parameter Estimates Affected by Sample Size (DT-HMFm)

ADD	π	μ	Λ	Ψ	B	C_{mis}
$(N, T) = (50, 10)$.057(.027)	.081(.012)	.077(.005)	.061(.010)	1.199 (.496)	.0029(.0022)
$(N, T) = (100, 10)$.038(.020)	.057(.008)	.053(.003)	.043(.006)	.648 (.226)	.0025(.0014)
$(N, T) = (200, 10)$.027(.014)	.040(.005)	.037(.002)	.030(.005)	.408 (.099)	.0023(.0010)
$(N, T) = (300, 10)$.022(.011)	.033(.004)	.031(.002)	.024(.004)	.340 (.083)	.0023(.0009)
$(N, T) = (700, 10)$.014(.008)	.021(.003)	.020(.001)	.016(.003)	.206(.043)	.0021(.0005)
$(N, T) = (200, 3)$.027(.014)	.074(.009)	.069(.004)	.056(.008)	1.422 (.607)	.0044(.0029)
$(N, T) = (200, 5)$.027(.014)	.058(.007)	.053(.003)	.043(.006)	.707 (.261)	.0028(.0017)
$(N, T) = (200, 10)$.027(.014)	.040(.005)	.037(.002)	.030(.005)	.408 (.099)	.0023(.0010)
$(N, T) = (200, 20)$.026(.014)	.029(.004)	.027(.002)	.021(.003)	.280 (.073)	.0018(.0007)
$(N, T) = (200, 200)$.027(.014)	.009(.001)	.009(.0005)	.006(.001)	.082(.020)	.0017(.0002)

Table S.7: Performance of Parameter Estimates Affected by Parameters (CT-HMFM)

ADD	π	μ	Λ	Ψ	B	C_{mis}
$\Psi = 1 * I$.026(.013)	.015(.002)	.014(.001)	.011(.002)	.120 (.027)	.0024(.0005)
$\Psi = .5 * I$.026(.013)	.012(.002)	.011(.001)	.005(.001)	.119(.027)	.0003(.0001)
$\Psi = .1 * I$.026(.013)	.010(.003)	.007(.001)	.001(.000)	.119(.027)	.0000(.0000)
μ : large diff	.026(.013)	.015(.002)	.014(.001)	.011(.002)	.120 (.027)	.002(.0005)
μ : medium diff	.027(.013)	.015(.001)	.015(.001)	.011(.002)	.124(.028)	.007(.001)
μ : minor diff	.034(.017)	.017(.003)	.478(.057)	.011(.002)	.161(.040)	.085(.004)
Λ : large diff	.026(.013)	.015(.002)	.014(.001)	.011(.002)	.120 (.027)	.002(.0005)
Λ : medium diff	.026(.013)	.014(.002)	.014(.001)	.011(.002)	.122(.029)	.006(.001)
Λ : minor diff	.026(.013)	.014(.002)	.014(.001)	.011(.002)	.122(.028)	.004(.001)
B : infreq transit	.026(.013)	.015(.002)	.014(.001)	.011(.002)	.120 (.027)	.002(.0005)
B : freq transit	.027(.013)	.015(.002)	.014(.001)	.011(.002)	.137(.043)	.007(.001)
$J = 2$.027(.021)	.012(.002)	.012(.001)	.011(.002)	.087 (.026)	.0015(.0003)
$J = 3$.026(.013)	.015(.002)	.014(.001)	.011(.002)	.120 (.027)	.0024(.0005)
$J = 4$.024(.011)	.017(.002)	.016(.001)	.011(.001)	.150(.028)	.0032(.0005)
$K = 2$.026(.013)	.015(.002)	.014(.001)	.010(.002)	.124 (.027)	.0069(.0008)
$K = 3$.026(.013)	.015(.002)	.014(.001)	.011(.002)	.120 (.027)	.0024(.0005)
$K = 5$.026(.013)	.015(.002)	.015(.001)	.012(.002)	.119(.027)	.0005(.0002)

Table S.8: Performance of Parameter Estimates Affected by Sample Size (CT-HMFM)

ADD	π	μ	Λ	Ψ	B	C_{mis}
$(N, T_i) = (50, [50, 100])$.052(.029)	.030(.004)	.028(.002)	.022(.003)	.254 (.058)	.0027(.0008)
$(N, T_i) = (100, [50, 100])$.042(.019)	.021(.003)	.020(.001)	.015(.002)	.175 (.038)	.0025(.0006)
$(N, T_i) = (200, [50, 100])$.026(.013)	.015(.002)	.014(.001)	.011(.002)	.120 (.027)	.0024(.0005)
$(N, T_i) = (500, [50, 100])$.018(.010)	.009(.001)	.009(.001)	.007(.001)	.076 (.017)	.0024(.0003)
$(N, T_i) = (200, [10, 30])$.029(.014)	.029(.004)	.027(.002)	.021(.004)	.251 (.061)	.0028(.0009)
$(N, T_i) = (200, [30, 50])$.027(.014)	.020(.003)	.019(.001)	.015(.003)	.180 (.043)	.0025(.0005)
$(N, T_i) = (200, [50, 100])$.026(.013)	.015(.002)	.014(.001)	.011(.002)	.120 (.027)	.0024(.0005)
$(N, T_i) = (200, [100, 150])$.028(.015)	.012(.001)	.011(.001)	.008(.001)	.098 (.021)	.0023(.0003)

E Additional Real Analysis Results

This section includes all the parameter estimates of the fitted model with $J = 3$ and $K = 8$.

In Table S.9, the estimated μ for each state is included. The estimated loading matrix for state 1 is listed in Table S.10, while that for state 2 and state 3 are listed in Table S.11 and Table S.12 respectively. In Table S.13, there are the parameter estimations of the transition model.

Table S.9: Estimated μ_j

μ_j	j=1	j=2	j=3
meanAcc	7.146	7.231	6.860
amplitude	3.906	3.913	3.621
SWCK	3.269	3.220	3.151
L5	3.765	3.800	3.555
NNmean.min	7.663	7.496	6.881
NNmean.mean	8.406	7.923	6.960
NNskew.q3	0.998	0.956	1.305
SDNN.max	7.284	6.571	6.246
SDNN.min	28.705	27.628	26.944
SDNN.mean	12.673	11.584	10.616
SDNN.var	20.014	19.333	18.512
lfhf.min	-4.393	-4.428	-4.829
lfhf.mean	-0.125	-0.046	-0.642
dc.min	3.888	3.168	2.706
dc.mean	7.423	6.453	5.418
SD1SD2.max	101.371	101.620	102.439
SD1SD2.min	26.001	25.885	26.745
SD1SD2.mean	1,703.646	1,703.711	1,704.842
SD1SD2.var	23.038	23.197	23.943
ApEn.max	4.320	3.813	3.975
ApEn.min	-2.694	-1.915	-2.280
ApEn.mean	1.901	1.596	1.146
ApEn.var	-4.546	-5.396	-4.782

Table S.10: Estimated Standardized Promax Factor Loading Matrix: State = 1 (Λ_1)

	0	1	2	3	4	5	6	7
meanAcc	-0.014	0.022	-0.013	-0.032	-0.989	-0.049	0.032	0.001
amplitude	0.011	0.023	0.004	0.046	-0.808	-0.017	-0.090	-0.066
SWCK	0.020	0.035	0.013	-0.168	0.435	0.039	0.214	0.057
L5	0.008	0.009	0.009	-0.126	-0.445	0.017	0.183	0.067
NNmean.min	0.002	0.109	-0.085	0.860	0.011	-0.065	0.189	0.097
NNmean.mean	0.187	0.278	0.100	0.752	-0.025	0.052	0.215	0.013
NNskew.q3	0.066	0.043	-0.122	-0.388	-0.009	-0.379	-0.354	0.062
SDNN.max	0.519	-0.007	0.028	0.097	0.053	0.267	-0.053	-0.057
SDNN.min	-0.052	-0.182	-0.133	0.280	0.004	-0.181	0.918	-0.252
SDNN.mean	.517	0.255	-0.068	-0.047	-0.004	-0.093	0.470	-0.162
SDNN.var	0.672	0.069	-0.010	-0.052	-0.069	0.469	-0.268	-0.036
lfhf.min	0.112	-0.115	-1.030	0.104	0.000	-0.048	0.175	0.217
lfhf.mean	0.000	0.017	-0.973	-0.046	-0.019	0.349	0.046	0.255
dc.min	-0.039	-0.146	-0.004	0.038	-0.038	0.185	0.164	-0.719
dc.mean	0.133	0.104	0.155	-0.148	0.015	-0.027	0.181	-0.929
SD1SD2.max	-0.014	-0.029	0.514	0.081	0.039	-0.062	0.045	0.489
SD1SD2.min	0.036	0.006	0.184	-0.003	-0.041	-0.787	0.150	0.088
SD1SD2.mean	0.095	-0.121	0.727	0.074	-0.002	-0.417	0.041	0.191
SD1SD2.var	0.058	-0.128	0.655	0.014	-0.050	0.346	-0.047	0.345
ApEn.max	0.106	-0.737	0.005	-0.334	0.019	-0.047	0.204	-0.007
ApEn.min	-0.991	0.024	0.012	-0.086	-0.030	0.163	0.103	-0.020
ApEn.mean	-0.472	-0.696	0.038	-0.160	0.011	0.117	0.053	-0.116
ApEn.var	1.063	-0.246	-0.024	-0.090	-0.030	-0.119	0.117	-0.017

Table S.11: Estimated Standardized Promax Factor Loading Matrix: State = 2 (Λ_2)

	0	1	2	3	4	5	6	7
meanAcc	-0.006	0.003	0.010	-0.034	0.938	-0.001	0.058	-0.232
amplitude	0.027	-0.034	0.005	0.038	0.860	-0.003	-0.015	-0.077
SWCK	-0.084	0.111	0.031	-0.130	-0.672	0.015	0.226	-0.084
L5	-0.062	0.079	-0.013	-0.141	0.128	0.042	0.142	-0.268
NNmean.min	-0.121	0.043	0.003	0.807	0.047	-0.043	-0.000	-0.035
NNmean.mean	-0.033	-0.055	-0.079	0.807	0.069	0.016	0.318	0.102
NNskew.q3	0.093	-0.185	0.114	-0.406	-0.093	-0.161	-0.099	-0.343
SDNN.max	0.019	-0.025	-0.197	0.063	-0.129	-0.097	0.600	-0.027
SDNN.min	0.638	0.345	0.188	0.253	-0.033	0.044	0.057	-0.048
SDNN.mean	0.530	-0.043	0.388	0.137	-0.040	0.089	0.663	0.045
SDNN.var	-0.100	-0.120	-0.010	0.057	0.037	0.013	0.862	-0.091
lfhf.min	-0.107	-0.117	0.869	0.111	-0.029	-0.158	-0.118	-0.154
lfhf.mean	-0.135	-0.029	0.980	-0.109	-0.026	0.087	-0.131	0.128
dc.min	0.473	0.148	-0.011	-0.082	0.110	-0.202	-0.047	0.069
dc.mean	0.770	-0.112	-0.058	-0.088	0.100	-0.318	0.283	0.129
SD1SD2.max	-0.038	-0.079	-0.212	0.072	-0.056	0.675	-0.093	0.003
SD1SD2.min	0.103	-0.061	-0.233	0.085	-0.035	-0.177	-0.291	-0.416
SD1SD2.mean	0.042	-0.044	-0.652	0.157	-0.041	0.263	-0.093	-0.287
SD1SD2.var	-0.077	-0.039	-0.171	-0.027	0.041	0.834	0.022	0.095
ApEn.max	0.837	-0.290	-0.094	-0.156	-0.022	0.208	-0.047	-0.029
ApEn.min	0.514	0.487	-0.024	-0.070	-0.026	0.059	-0.250	-0.091
ApEn.mean	0.932	0.070	-0.230	-0.047	-0.019	0.024	-0.033	-0.040
ApEn.var	0.002	-0.972	0.091	-0.069	0.098	0.096	0.114	0.037

Table S.12: Estimated Standardized Promax Factor Loading Matrix: State = 3 (Λ_3)

	0	1	2	3	4	5	6	7
meanAcc	0.008	-0.008	0.010	-0.041	-0.989	0.004	0.049	0.159
amplitude	0.010	0.001	0.090	0.007	-0.725	0.025	-0.053	0.380
SWCK	-0.003	-0.086	0.099	-0.132	0.106	0.008	0.165	-0.560
L5	0.009	-0.040	-0.065	-0.058	-0.609	-0.018	0.095	-0.261
NNmean.min	0.026	-0.034	-0.078	0.686	0.047	-0.133	0.056	0.005
NNmean.mean	-0.092	-0.041	0.007	0.869	0.013	0.007	0.230	0.154
NNskew.q3	-0.050	-0.044	-0.007	-0.533	-0.018	-0.061	0.327	-0.218
SDNN.max	0.066	0.010	-0.130	-0.028	0.024	-0.096	0.668	-0.174
SDNN.min	-0.780	-0.344	0.061	0.103	-0.005	0.059	-0.071	-0.096
SDNN.mean	-0.798	0.048	0.286	0.227	-0.048	0.155	0.378	-0.086
SDNN.var	-0.069	0.120	-0.019	0.134	-0.105	0.033	0.945	-0.045
lfhf.min	0.049	0.082	0.968	0.062	-0.040	-0.180	-0.181	-0.271
lfhf.mean	0.017	0.005	1.073	-0.108	-0.007	0.040	-0.139	-0.069
dc.min	-0.408	-0.034	-0.077	-0.125	0.005	-0.189	-0.118	0.171
dc.mean	-0.750	0.049	-0.099	-0.007	0.028	-0.171	0.274	0.223
SD1SD2.max	0.035	0.026	-0.282	0.011	0.007	0.585	-0.094	-0.105
SD1SD2.min	-0.122	0.112	-0.295	0.117	-0.081	-0.198	-0.333	-0.356
SD1SD2.mean	0.053	0.070	-0.610	0.054	-0.019	0.227	-0.126	-0.244
SD1SD2.var	-0.027	-0.039	-0.158	-0.134	-0.009	0.925	-0.042	0.095
ApEn.max	-0.837	0.490	0.018	-0.150	0.047	0.081	-0.086	-0.013
ApEn.min	-0.801	-0.357	-0.038	-0.013	-0.002	0.003	-0.157	-0.090
ApEn.mean	-1.009	0.041	-0.079	0.029	0.003	0.077	-0.021	-0.117
ApEn.var	0.256	0.971	0.021	-0.027	0.028	-0.024	0.127	0.152

Table S.13: Estimated Transition Model (\mathbf{B}_{kj})

j	\mathbf{B}_{1j0}	\mathbf{B}_{1j1}	\mathbf{B}_{1j2}	\mathbf{B}_{2j0}	\mathbf{B}_{2j1}	\mathbf{B}_{2j2}	\mathbf{B}_{3j0}	\mathbf{B}_{3j1}	\mathbf{B}_{3j2}
1	-	-	-	-0.462	-0.243	-0.019	-2.430	-0.233	-0.018
2	-1.736	-0.091	0.017	-	-	-	0.334	-0.759	-0.021
3	-5.046	1.426	0.015	-1.723	0.053	0.005	-	-	-

F Flash Survey Data

The Mindstrong Discovery™ application on participants’ smart phones was used to deliver brief questionnaires (i.e., flash surveys). Participants were asked to reply to these questions every day for the first week of the research, then every other day until week 12, and then weekly after that.

Based on the RDoC framework, ten latent constructs associated with APNS were developed using flash survey items selected by domain experts: Pain, Loss, Sleep Discontinuity, Nightmare, Somatic Symptoms, Mental Fatigue, Avoidance, Re-experience, and Anxious. For each of the ten constructs, scores were generated for each participant, utilizing the flash survey questions. The higher the score of the construct, the more severe the symptom. While most construct scores range from -1 to 5 , the score range for mental fatigue and somatic symptoms is $(0, 12)$, and the range of the pain construct score is $(-1, 10)$. In the analysis, we only consider observations for each individual whose estimated states are known on the same day that they submit their survey responses. In the analysis, original observations for each feature are scaled to be in the range of $[0, 1]$.